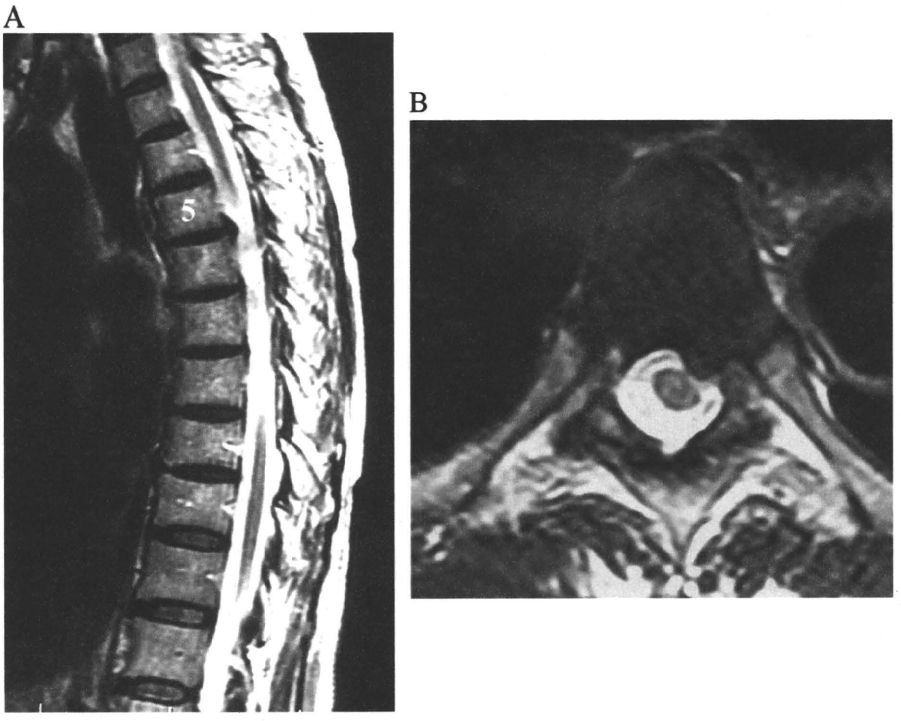

Figure 2. A 62-year-old woman with posterior disc protrusion and spinal cord compression at T5–T6. **A**, T2 sagittal image. **B**, T2 axial image demonstrating that the spinal cord is slightly compressed by disc herniation on the left side.

normalities detected on the MRI images included ossification of the ligamentum flavum in 2 subjects, Schmorl nodules in 2 subjects, and the enlargement of the central canal of the spinal cord in 1 subject. Kappa scores were 0.60 for decrease in the signal intensity of the discs, 0.82 for posterior disc protrusion, 0.75 for anterior compression of the dural sac, and 0.57 for disc space narrowing, indicating that the interobserver reliability of MRI reading was good to excellent.

Comparison Between Cervical and Thoracic Spine

Eighty-five (90.4%) subjects exhibited positive MRI findings, indicating degeneration at 1 or more intervertebral levels in the cervical spine (Table 3). The percentages of subjects with a positive finding at 1 or more intervertebral disc levels of the cervical spine were as follows: 80.9% exhibited a decrease in the signal intensity of the discs, 76.6% exhibited posterior disc protrusion, 80.9% exhibited anterior compression of the dural sac, and 34.0% exhibited disc space narrowing. Thus, a decrease in the signal intensity of the discs, posterior disc protrusion, and anterior compression of the dura were observed significantly more frequent in the cervical than in the thoracic spine ($P < 0.05$).

Table 3. The Percentage of the Subjects Who Had Positive MRI Findings at 1 or More Intervertebral Discs

	Cervical Spine	Thoracic Spine	*P**
Decrease in signal intensity of discs	80.9	37.2	0.02
Posterior disc protrusion	76.6	30.9	0.05
Anterior compression of dura	80.9	29.8	0.03
Disc space narrowing	34.0	4.3	0.11
Any 1 of the 4 findings	90.4	46.8	0.12

Factors Associated With Degenerative MRI Findings

A decrease in the signal intensity of the discs was significantly associated with age (odds ratio [OR], 11.21; 95% confidence interval [CI], 2.70–46.5; $P = 0.001$); posterior disc protrusion was significantly associated with age (OR, 3.44; 95% CI, 1.02–16.61; $P = 0.046$), smoking habit (OR, 4.94; 95% CI, 1.55–15.71; $P = 0.007$), and presence of posterior disc protrusion in the cervical spine (OR, 4.25; 95% CI, 1.01–17.92; $P = 0.048$); and anterior compression of the dura was significantly associated with smoking habit (OR, 3.99; 95% CI, 1.28–12.44; $P = 0.017$), whereas disc space narrowing was not associated with any of the factors (Table 4).

■ Discussion

This study revealed that approximately half (46.8%) of the asymptomatic individuals with a mean age of 48 years exhibited positive MRI findings indicating degeneration at 1 or more intervertebral levels of the thoracic spine. The positive rates of each MRI finding increased with age, suggesting that these positive MRI findings represent age-related degeneration of the intervertebral discs. Degenerative MRI findings in the thoracic spine were rarer than those in the cervical spine (90.4%); in particular, a decrease in the signal intensity of the intervertebral discs (37.2% *vs.* 80.9%), posterior disc protrusion (30.9% *vs.* 76.6%), and anterior compression of the dura (29.8% *vs.* 80.9%) were significantly less frequent in the thoracic than in the cervical spine. Several factors that were significantly associated with tho-

Table 4. Relationships Between Degenerative MRI Findings and Factors

Factors	No. Patients	Decrease in Signal Intensity	Posterior Disc Protrusion	Anterior Compression of Dura	Disc Space Narrowing
Age					
<40	28	3 (10.7)*	6 (21.4)*	6 (21.4)	1 (3.6)
≥40	66	32 (48.5)	23 (34.8)	22 (33.3)	3 (4.5)
Sex					
Male	48	16 (33.3)	17 (35.4)	16 (33.3)	3 (6.3)
Female	46	19 (41.3)	12 (26.1)	12 (26.1)	1 (2.2)
Smoking					
Smoker	21	8 (38.1)	11 (52.4)*	10 (47.6)*	1 (4.8)
Nonsmoker	73	27 (37.0)	18 (24.7)	18 (24.7)	3 (4.1)
Sports					
Regularly	16	6 (37.5)	6 (27.5)	6 (37.5)	2 (12.5)
None	78	29 (37.2)	23 (29.5)	22 (28.2)	2 (2.6)
BMI					
<25.0	69	26 (37.7)	19 (27.5)	19 (27.5)	3 (4.3)
≥25.0	25	9 (36.0)	10 (40.0)	9 (36.0)	1 (4.0)
MRI finding in cervical spine†					
Positive		33/76 (43.4)	26/72 (36.1)*	27/76 (35.5)*	3/32 (9.4)
Negative		2/18 (11.1)	3/22 (13.6)	1/18 (5.6)	1/62 (1.6)

Values in parentheses are percentage values.
*$P < 0.05$ (logistic regression analysis).
†MRI finding in the cervical spine corresponding to that in the thoracic spine in the rows.

racic disc degeneration were age, smoking habit, and the presence of cervical disc degeneration. Smoking has been reported to promote disc degeneration in previous basic and clinical studies.[19,20] For example, Battie *et al*[19] studied pairs of identical twins with a high discordance in cigarette smoking habit and found that the mean disc degeneration score for the lumbar spine was 18% higher in the smokers than in the nonsmokers. Thoracic intervertebral discs, which are less exposed to mechanical stress than the cervical and lumbar intervertebral discs, might also be affected by the detrimental effects of nicotine, similar to the lumbar intervertebral discs.

The presence of posterior disc protrusion and anterior compression of the dura in the cervical spine were significantly related to these parameters in the thoracic spine, indicating that structural deterioration of the intervertebral discs can occur simultaneously in the cervical and thoracic spine, as has often been reported for the cervical and lumbar spine.[21] Thus, spine surgeons should carefully determine the affected level responsible for, with multilevel lesions.

To date, several imaging studies on degenerative changes in the thoracic spine have been performed. Williams *et al*[16] reviewed T1-weighted sagittal MR images of the thoracic spine obtained in 48 oncology patients and found an unexpectedly high prevalence of thoracic disc herniation (14.5%). In another study by Wood *et al*,[14] 73% of 90 asymptomatic subjects exhibited positive anatomic findings at 1 or more levels, including disc herniation in 37%, bulging of a disc in 58%, deformation of the spinal cord in 29%, and endplate irregularities in 38%. Compared with this previous study, the prevalence of asymptomatic disc abnormalities was lower in our study. In particular, a remarkable difference was observed in the prevalence of endplates irregularities and spinal cord deformation. Only 2 subjects with endplate irregularities and 2 with spinal cord compression were observed in this study. These differences in the prevalences of the MRI findings may be attributable to differences in age, sex, ethnicity, diagnostic criteria, and MRI protocols between the 2 studies. Moreover, in the study by Wood *et al*, 30 volunteers with lower back pain but without pain in the thoracic spine were included in the analysis, whereas all the subjects with pain in the neck or lower back were excluded in this study. Nonetheless, both studies delineated a relatively high prevalence of positive MRI findings, indicating degeneration in the thoracic spine, even in an asymptomatic population.

Awwad *et al*[17] reviewed postmyelography computed tomographic scans of 68 asymptomatic herniated thoracic discs and compared them with 5 symptomatic herniated discs but could not identify any imaging feature that could reliably differentiate symptomatic discs from asymptomatic ones. Wood *et al*[22] followed 20 subjects with 48 asymptomatic thoracic herniations for a mean follow-up period of 26 months. All subjects remained asymptomatic during the follow-up period, and the disc herniations exhibited little change in size; in fact, large herniations tended to have decreased in size at the time of the follow-up examination. Thus, thoracic disc herniations or protrusions are not rare in asymptomatic subjects,[11,22,23] and differentiation between asymptomatic and symptomatic disc herniations or protrusions using MRI is not easy. Considering the technical complexity and invasiveness of surgery for thoracic intervertebral disc lesions, disc abnormalities detected on MRI should be carefully evaluated whether they are responsible for the patients' symptoms, by a meticulous neurologic examination and other diagnostic methods, such as a myelogram and provocative discography, before determining the indication for surgery.[24]

One of the limitations of this study was a possible bias in the study population. The majority of the participants were white-collared workers, rather than manual laborers; therefore, the participants may not exactly represent the general population. Nonetheless, this is the first report describing degenerative changes in the thoracic spine in asymptomatic subjects and comparing these changes with those in the cervical spine. The information obtained in this study could be used as a norm when evaluating MRI findings of the thoracic spine in patients with thoracic spinal disorders.

■ Key Points

- Magnetic resonance imaging (MRI) study was undertaken to investigate the incidence of degenerative MRI findings of the thoracic spine in asymptomatic subjects and to identify factors related to the degeneration of the thoracic discs.

- Ninety-four asymptomatic volunteers (48 men and 46 women, mean age of 48.0 ± 13.4 years) underwent MRI of the thoracic and cervical spine.
- The following 4 MR findings related to intervertebral disc degeneration were evaluated using a numerical grading system: (1) decrease in the signal intensity of the intervertebral discs (DSI), (2) posterior disc protrusion (PDP), (3) anterior compression of the dural sac (ACD), and (4) disc space narrowing (DSN).
- Degenerative MRI findings at 1 or more intervertebral levels in the thoracic spine were positive in 44 (46.8%) subjects. The percentages of the subjects with positive MRI findings were 37.2% in DSI, 30.9% in PDP, 29.8% in ACD, and 4.3% in DSN.
- DSI was significantly associated with age; PDP with age, smoking, and presence of PDP in the cervical spine; and ACD was associated with smoking.

Acknowledgment

The authors thank Mr. Toshio Watanabe at the Central Radiotechnology Department of Keio University Hospital, for his cooperation in this study.

References

1. Yasuma T, Koh S, Okamura T, et al. Histological changes in aging lumbar intervertebral discs. Their role in protrusions and prolapses. *J Bone Joint Surg Am* 1990;72:220–9.
2. Gore DR, Sepic SB, Gardner GM. Roentgenographic findings of the cervical spine in asymptomatic people. *Spine* 1986;11:521–4.
3. Boden SD, McCowin PR, Davis DO, et al. Abnormal magnetic-resonance scans of the cervical spine in asymptomatic subjects. A prospective investigation. *J Bone Joint Surg Am* 1990;72:1178–84.
4. Boden SD, Davis DO, Dina TS, et al. Abnormal magnetic-resonance scans of the lumbar spine in asymptomatic subjects. A prospective investigation. *J Bone Joint Surg Am* 1990;72:403–8.
5. Lehto IJ, Tertti MO, Komu ME, et al. Age-related MRI changes at 0.1 T in cervical discs in asymptomatic subjects. *Neuroradiology* 1994;36:49–53.
6. Matsumoto M, Fujimura Y, Suzuki N, et al. MRI of cervical intervertebral discs in asymptomatic subjects. *J Bone Joint Surg Br* 1998;80:19–24.
7. Jensen MC, Brant-Zawadzki MN, Obuchowski N, et al. Magnetic resonance imaging of the lumbar spine in people without back pain. *N Engl J Med* 1994;331:69–73.
8. Leboeuf-Yde C, Nielsen J, Kyvik KO, et al. Pain in the lumbar, thoracic or cervical regions: do age and gender matter? A population-based study of 34,902 Danish twins 20–71 years of age. *BMC Musculoskelet Disord* 2009; 10:39.
9. Mio F, Hirose Y, Chiba K, et al. A functional polymorphism in COL11A1, which encodes the a1 chain of type XI collagen, is associated with susceptibility to lumbar disc herniation. *Am J Hum Genet* 2007;81:1271–7.
10. Okada E, Matsumoto M, Ichihara D, et al. Aging of the cervical spine in healthy volunteers: a 10-year longitudinal magnetic resonance imaging study. *Spine* 2009;34:706–12.
11. McInerney J, Ball PA. The pathophysiology of thoracic disc disease. *Neurosurg Focus* 2000;9:e1.
12. Aizawa T, Sato T, Tanaka Y, et al. Thoracic myelopathy in Japan: epidemiological retrospective study in Miyagi Prefecture during 15 years. *Tohoku J Exp Med* 2006;210:199–208.
13. Otani K, Yoshida M, Fujii E, et al. Thoracic disc herniation. Surgical treatment in 23 patients. *Spine* 1988;13:1262–7.
14. Wood KB, Garvey TA, Gundry C, et al. Magnetic resonance imaging of the thoracic spine. Evaluation of asymptomatic individuals. *J Bone Joint Surg Am* 1995;77:1631–8.
15. Arana E, Martí-Bonmatí L, Mollá E, et al. Upper thoracic-spine disc degeneration in patients with cervical pain. *Skeletal Radiol* 2004;33:29–33.
16. Williams MP, Cherryman GR, Husband JE. Significance of thoracic disc herniation demonstrated by MR imaging. *J Comput Assist Tomogr* 1989; 13:211–4.
17. Awwad EE, Martin DS, Smith KR Jr, et al. Asymptomatic versus symptomatic herniated thoracic discs: their frequency and characteristics as detected by computed tomography after myelography. *Neurosurgery* 1991;28: 180–6.
18. Landis JR, Koch GG. The measurement of observer agreement for categorical data. *Biometrics* 1977;33:159–74.
19. Battié MC, Videman T, Gill K, et al. Smoking and lumbar intervertebral disc degeneration: an MRI study of identical twins. *Spine* 1991;16:1015–21.
20. Akmal M, Kesani A, Anand B, et al. Effect of nicotine on spinal disc cells: a cellular mechanism for disc degeneration. *Spine* 2004;29:568–75.
21. Jacobs B, Ghelman B, Marchisello P. Coexistence of cervical and lumbar disc disease. *Spine* 1990;15:1261–4.
22. Wood KB, Blair JM, Aepple DM, et al. The natural history of asymptomatic thoracic disc herniations. *Spine* 1997;22:525–30.
23. Brown CW, Deffer PA, Akmakjian J, et al. The natural history of thoracic disc herniation. *Spine* 1992;175:97–102.
24. Wood KB, Schellhas KP, Garvey TA, et al. Thoracic discography in healthy individuals. A controlled prospective study of magnetic resonance imaging and discography in asymptomatic and symptomatic individuals. *Spine* 1999; 24:1548–55.

SPINE Volume 35, Number 11, pp E505–E509

Complicated Surgical Resection of Malignant Tumors in the Upper Cervical Spine After Failed Ion-Beam Radiation Therapy

Morio Matsumoto, MD,* Kota Watanabe, MD,† Ken Ishii, MD,* Takashi Tsuji, MD,* Hironari Takaishi, MD,* Masaya Nakamura, MD,* Yoshiaki Toyama, MD,* Kazuhiro Chiba, MD,* Yorihisa Imanishi, MD,‡ Kazuo Kishi, MD,§ and Hiromasa Kawana, DDS, PhD¶

Study Design. Case report.

Objective. To report 3 cases of malignant tumors in the upper cervical spine that were treated surgically by a combination of posterior tumor resection and stabilization and anterior tumor resection through a mandible-splitting approach after failed ion-beam radiation therapy.

Summary of Background Data. Few clinical reports have described in detail the postoperative complications associated with transoral surgical resection of tumors in the upper cervical spine after unsuccessful ion-beam radiation therapy.

Methods. Three patients with malignant tumors in the upper cervical spine who had undergone ion-beam radiotherapy and experienced tumor recurrence were treated by a combination of posterior and anterior surgery through a mandible-splitting approach. One patient (patient 1, a 32-year-old man) had a hemangioendothelioma at the C2 and C3 level, whereas the other 2 patients (patient 2, a 66-year-old woman and patient 3, a 65-year-old man) had a chordoma at the C2 and C3 level.

Results. The intralesional but macroscopic total resection of the tumors was achieved in all 3 patients. However, serious complications developed after surgery, including deep wound infection, cerebrospinal fluid leakage, and meningitis in patient 1, prolonged swallowing difficulty, subsidence of the strut graft, and recurrence in patient 2, and deep wound infection and discitis causing progressive paralysis in patient 3. All patients underwent salvage surgery, including debridement of the wound in patient 1, posterior reinforcement using instrumentation and posterior tumor resection for the recurrent tumor in patient 2, and anterior debridement of the wound with a pedicle flap using the pectoral major muscle in patient 3 to address these problems. Patients 1 and 3 had no signs of recurrence at the time of a follow-up examination.

Conclusion. Severe complications, mainly associated with the disturbance in healing of the retropharyngeal wall, were observed in all 3 patients. A preventive method, such as primary repair of the retropharyngeal wall using muscular/musculocutaneous flaps, should be considered for patients undergoing resection through a transoral approach after ion-beam irradiation.

Key words: chordoma, epithelioid hemangioendothelioma, upper cervical spine, ion-beam radiotherapy, mandible-splitting approach. **Spine 2010;35:E505–E509**

Malignant primary tumors, including chordoma and other rare sarcomas, occasionally arise in the upper cervical spine. Treatment options for these slow-growing malignant tumors are radical excision, radiotherapy, and a combination of both. Because of limited access to the lesions as a result of the close vicinity of critical structures, including the spinal cord and vertebral arteries, radiation therapy followed by a diagnostic biopsy, rather than excision, is often chosen as the primary treatment. Recent advance in stereotactic radiotherapy and ion-beam radiotherapy have made this therapeutic strategy more popular.[1,2] Noël et al[1] reported 100 consecutive patients with a chordoma at the base of the skull or in the upper cervical spine who were treated using a combination of high-energy photons and protons. The 2- and 4-year local control rates were 86.3% and 53.8%, respectively, indicating that radiation therapy might not always be effective for patients with malignant tumors in the upper cervical spine region. For patients with recurrences after radiation therapy, surgical resection might be the last resort or various life-threatening problems including pain, paralysis, difficulties in respiration, and swallowing caused by tumor regrowth could develop. The surgical treatment of spine tumors after irradiation is known to be associated with a higher complication rate[3,4] and could be more so in the upper cervical spine.

In this study, we report 3 patients with malignant tumors in the upper cervical spine who were treated surgically by a combination of posterior tumor resection and stabilization and anterior tumor resection through a mandible-splitting approach after failed ion-beam radiation therapy.

From the Departments of *Orthopaedic Surgery, †Advanced Therapy for Spine and Spinal Cord Disorders, ‡Oto-Rhino-Laryngology, §Plastic and Reconstruction Surgery, and ¶Dentistry and Oral Surgery, School of Medicine, Keio University, Tokyo, Japan.

Acknowledgment date: June 15, 2009. Revision date: September 24, 2009. Acceptance date: October 31, 2009.

The manuscript submitted does not contain information about medical device(s)/drug(s).

No funds were received in support of this work. No benefits in any form have been or will be received from a commercial party related directly or indirectly to the subject of this manuscript.

Address correspondence and reprint requests to Morio Matsumoto, MD, Department of Orthopaedic Surgery, School of Medicine, Keio University, 35 Shinanomachi, Shinjuku-ku, Tokyo, 160-8582, Japan; E-mail: morio@sc.itc.keio.ac.jp

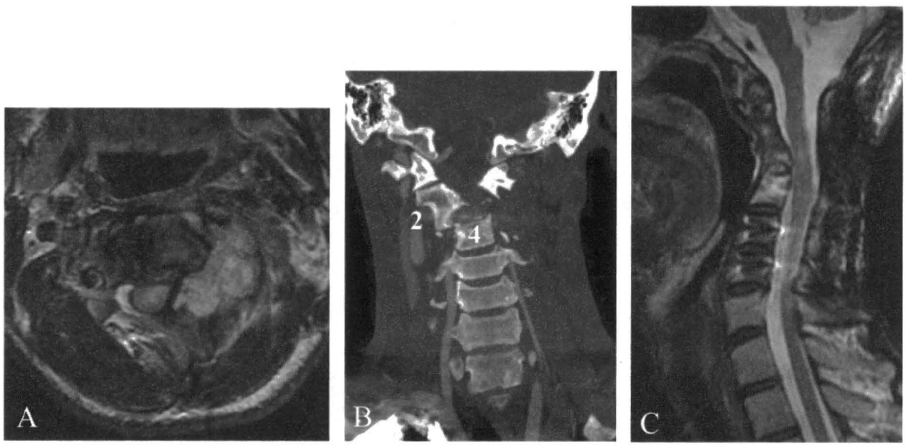

Figure 1. Patient 1, with a hemangioendothelioma at C2 and C3. **A**, Preoperative MRI T2-weighted axial image demonstrating a high-intensity tumor on the left side. **B**, Reconstruction angio-computed tomography demonstrating destructive changes in C2 and C3. **C**, MRI T2-weighted sagittal image obtained 1½ years after surgery shows good decompression of the spinal cord and no signs of tumor recurrence.

■ Materials and Methods

Three patients with primary malignant tumors in the upper cervical spine were referred to our hospital for the treatment of recurrences after unsuccessful ion-beam radiation therapy. All patients had undergone an open biopsy through a posterior approach. One patient (patient 1) had an epithelioid hemangioendothelioma, and 2 patients (patients 2 and 3) had chordomas. Patient 2 had undergone a posterior occipitocervical fusion using a lateral mass screw system at the time of the open biopsy. Patient 3 had undergone posterior decompression surgery twice by laminoplasty and a laminectomy for the treatment of cervical myelopathy caused by the compression of the spinal cord by the tumor.

Surgical Procedures

The surgical procedures were almost identical among the 3 patients, with some modifications depending on the localization of the tumor, the severity of the tissue destruction, and previous surgical procedures.

Surgery was conducted using a combined posterior and anterior approach. Patients were placed in a prone position with their heads fixed by a Mayfield device. The posterior aspects of the occiput and cervical spine were exposed through a midline incision. The laminae and facet joints were removed using a high-speed diamond burr to decompress the spinal cord and to expose the posterior aspect of the tumors. The bilateral vertebral arteries were identified; and one on the tumor side was ligated in 2 patients (patient 1, 3) and was preserved in 1 patient (patient 2). Silicon sheets were placed ventrally to the preserved vertebral arteries, so that the arteries would be easily identified during the subsequent anterior procedure. The C2 and C3 nerve roots on the tumor side were severed. The posterior and lateral portions of the tumor including the pseudocapsule were resected as completely as possible using a CUSA from the posterior approach. Pieces of Gelfoam were packed into the space created after the tumor resection to control bleeding and to act as a landmark for the posterior margin during the subsequent anterior tumor resection. Thereafter, posterior reconstruction of the cervical spine was performed using occipitocervical fixation devices, except in patient 2 who had undergone this procedure at the previous hospital. Pedicle screws and/or lateral mass screws were used for anchors to the cervical spine. An autologous bone from the posterior iliac crest was grafted.

After the completion of the posterior procedures, the patients were flipped to a supine position, and a tracheostomy was created. Dentistry and oral surgeons exposed the mandible. In patients 1 and 3, whose tumors were located at the C3 level or above, the lower lip and tongue were spared, and the mucosa of the oral cavity was incised using a scalpel; the periosteum was then stripped off from the anterior aspect of the mandible. Then, the mandible was split in the midline using a micro bone-saw. In patient 2, because the tumor had extended to an extreme lateral, the lower lip and tongue were also split along with the mandible to allow a wider surgical view. The soft palate was also split in the middle to obtain access to the clivus for strut grafting in patient 2 and 3.

The mucosa and submucosal muscles in the retropharynx were then divided using a scalpel, and a Crockard retractor was placed. Under a surgical microscope, the anterior arch of the atlas and odontoid process were removed using a diamond burr. Macroscopically, the total resection of the tumor in the C2 and C3 vertebral bodies and the tumor's extraosseous portion was conducted using a fine diamond burr and CUSA. Identification of the Gelfoam placed during the posterior procedures was the indication of the complete resection. After the total resection of the tumor, an anterior strut obtained from the fibula or iliac crest was grafted from the clivus to the C3 or C4 vertebral body. The meticulous primary suturing of the retropharyngeal mucosa and muscles was conducted by otolaryngologists, and the split mandible was reconstructed using a mandible plate by the dentistry and oral surgeons.

After surgery, a ventilator was used for 1 or 2 days until the patients' voluntary respiration stabilized. Intravenous hyperalimentation followed by enteral nutrition was administered until the retropharyngeal mucosa healed, and the patients were able to swallow smoothly after intensive swallowing rehabilitation.

Clinical Course of Patients

The clinical course of each patient is described in detail later.

Patient 1. A 32-year-old man experienced the onset of numbness in his left upper extremity (Figure 1). At a previous hospital, a computed tomography-guided biopsy was conducted, which established the diagnosis of epithelioid hemangioendothelioma. The patient underwent carbon-ion radiotherapy (dose, 60 Grays), which turned out to be ineffective, and the tumor continued to grow. He was referred to our hospital for further treatment 11 months after the radiotherapy.

Neurologically, the patient exhibited hyperreflexia and motor weakness in his left side and could barely walk with

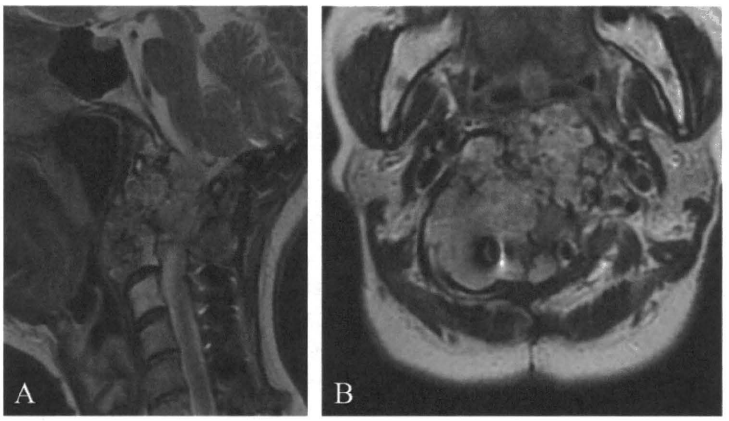

Figure 2. Patient 2, with a chordoma at C2 and C3. **A**, MRI T2-weighted sagittal image obtained before surgery. **B**, MRI T2-weighted axial image obtained before surgery showing that the tumor had extended widely, particularly on the right side and had completely surrounded a titanium rod and the vertebral artery on the right side.

crutches. Radiographs, computed tomography, and magnetic resonance imaging (MRI) examinations demonstrated destructive changes and the tumor involvement of C2 and C3, mainly on the left side. Angiography revealed the high vascularity of the tumor, and embolization of the feeders using polyvinyl alcohol was performed.

The patient underwent a posterior tumor resection and fusion from the occiput to C6 using a cervical pedicle screw system with a bone graft from the posterior iliac crest, followed by anterior tumor resection. The gross total resection of the tumor was achieved. The total surgical time was 15 hours, and the estimated blood loss was 350 mL.

After surgery, the patient developed a deep wound infection and cerebrospinal fluid leakage into the esophagus, which lasted for 4 weeks after the surgery. The patient also developed aspiration pneumonia and mild meningitis, possibly because of the continuous leakage of cerebrospinal fluid. Because the administration of antibiotics was ineffective for controlling the infection, posterior wound debridement was performed. During the revision surgery, iodine contrast medium that had been injected into the posterior wound passed into the esophagus through the unhealed retropharyngeal wall.

After the revision surgery and the continuous administration of antibiotics, the infection and leakage of cerebrospinal fluid subsided, and the defect in the retropharyngeal mucosa closed spontaneously. The patient resumed an oral diet 12 weeks after surgery. At a 2-year follow-up examination, the patient was free from disease. The patient had no neurologic deficits other than a mild numbness on his left arm and leg.

Patient 2. A 66-year-old woman underwent an occipitocervical fusion using a lateral mass screw system and proton-beam radiation (65 Grays) after an open biopsy at a previous hospital, which established the diagnosis of a chordoma (Figure 2). The tumor continued to grow even after the radiation therapy, and the patient was referred to our hospital for further treatment 23 months after the radiation therapy. She had numbness and a sensory disturbance in her right upper extremity but could walk without difficulty. During posterior procedures, the rod was retrieved before the tumor resection, and the gross total resection of the posterolateral part of the tumor was achieved while preserving the right vertebral artery. During the anterior approach, a small laceration of the right vertebral artery occurred, but the bleeding was successfully controlled using Aviten and Gelfoam. The anterior part of the tumor was resected using CUSA, enabling a gross total resection of the tumor. The total surgical time was 18 hours and 10 minutes, and the estimated blood loss was 3223 mL.

After the surgery, the patient developed dysphasia lasting for 3 months as a result of the delayed healing of the retropharyngeal mucosa. She also experienced a sinking of the strut graft, which was salvaged by the addition of posterior instrumentation and fusion at 8 weeks after the initial surgery. Unfortunately, tumor recurrence was detected on MRI at 15 months after the surgery, and palliative posterior decompression was performed for progressive right hemiparesis.

Patient 3. A 65-year-old man underwent an open biopsy through a posterior midline incision, revealing the tumor to be a chordoma, followed by laminoplasty and a partial resection of the tumor and carbon-beam radiotherapy (total dose, 60 Grays), but he developed a recurrence at 10 months after the radiation therapy (Figure 3). Although he underwent a partial resection of the recurrent tumor again through a posterolateral approach on the left side, the tumor recurred again 8 months later, and he was referred to our hospital for further treatment.

Neurologically, he had weakness in his left upper and lower extremities and could barely walk with a crutch. He also had bladder and bowel dysfunction. After embolization of the vertebral artery on the left side using platinum wires, he underwent a combined posterior and anterior tumor resection surgery.

During the posterior procedures, adhesive scar tissue that was difficult to dissect was found between the dura and the tumor. Therefore, the plane between the outer and inner layers of the dura was used for the dissection, and the outer layer was resected with the tumor.[5] A posterolateral portion of the tumor was resected using CUSA, with the left C3 spinal nerve root. The tumor around the vertebral artery, which was embolized before surgery, was completely resected. Occipitocervical stabilization was conducted using pedicle screws on the left side (embolization side) only. Lateral mass screws were used on the right side to avoid injuring the remaining vertebral artery. After the gross total removal of the tumor from an anterior approach, a tricortical iliac bone graft was placed from the clivus to C3. The total surgical time was 14 hours and 10 minutes, and the estimated blood loss was 650 mL.

The patient developed a breakdown of the posterior retropharyngeal wall, resulting in the development of a long-lasting infection in the dead space that was created by the tumor resection. Controls of the infection were attempted using broad-spectrum antibiotics and the placement of a percutaneous en-

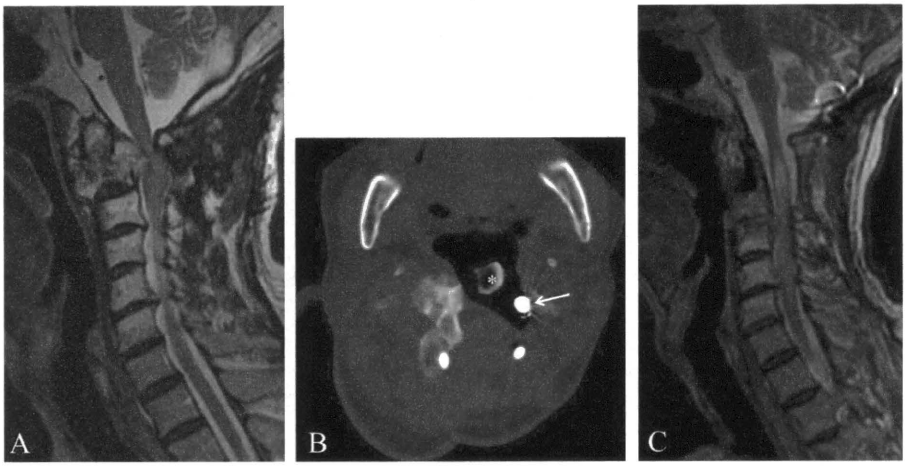

Figure 3. Patient 3, with chordoma at C2. **A**, Preoperative MRI T2-weighted sagittal image. **B**, Postoperative computed tomography showing a large cavity communicating between the pharynx and the epidural space. (Asterisk: iliac crest graft and arrow: embolization coils in the left vertebral artery.) **C**, Postoperative MRI T2-weighted sagittal image showing discitis and an epidural abscess at C3–C4 and a multilevel intramedullary high-intensity lesion in the spinal cord.

doscopic gastrostomy to avoid contamination during oral feeding. However, 7 months later, the patient developed progressive left hemiparesis with a high fever and elevated C-reactive protein level. An MRI examination revealed discitis and an epidural abscess at the C3–C4 level. After the failure of conservative therapy and a progression of neurologic deterioration resulting in an inability to walk, he underwent debridement of the infected C3 vertebral body, C3–C4 disc, and epidural abscess with retrieval of the infected iliac crest graft. After the completion of the debridement, the retropharyngeal dead space was covered using a reversed pectoral major muscle pedicle flap.

The infection subsided and the patient improved neurologically, becoming ambulatory with a T-cane. At a 1-year follow-up examination, he still could not swallow smoothly and continued to receive enteral nutrition through his gastrostomy.

■ Discussion

For slow-growing malignant tumors in the upper cervical spine, aggressive total surgical resection is paramount to obtain curability. For this purpose, a combined posterior and anterior or lateral approach has been used and reported in previous studies.[6–10] For the anterior approach, several surgical options can be used, including a bilateral high anterior cervical approach, an anterior midline transoral with/without transpalatine approach, and a mandible-splitting approach combined with a transglossal or circumglossal approach.[7,9,11] For tumors extending widely beyond the lateral margin of the transverse processes, the splitting of the mandible in addition to the transoral approach is necessary to obtain a sufficient surgical view. If a wide exposure of C3 and C4 is necessary, the tongue should also be divided along the midline.

Boriani *et al*[12] reported the results of a retrospective study of 52 cases with a chordoma in the mobile spine; in this series, 12 of 16 cases treated with intralesional and extracapsular excision followed by radiation therapy developed recurrences, whereas 12 of 18 patients treated with an *en bloc* resection were continuously disease free after an average of 8 years. Rhines *et al*[9] reported a case of multilevel cervical chordoma with C-2 involvement that was successfully treated using a 2-staged *en bloc* resection procedure. Thus, *en bloc* resection is preferable in terms of curability; however, in most cases with upper cervical involvement, an *en bloc* resection is too technically demanding, with an intralesional subtotal or total resection being a more realistic, as have been reported by most previous authors.[7,10]

Epithelioid hemangioendothelioma, as seen in patient 1, is a very rare spinal tumor arising from endothelial cells.[13,14] Because of the limited number of reported cases of the upper cervical spine, the effectiveness of surgical management and radiotherapy remains to be clarified. Aquilina *et al*[13] reported a 60-year-old male patient with involvement of the C2–C4 vertebrae who was treated with posterior occipitocervical fusion followed by radiotherapy. Resection surgery was not conducted because the authors thought that the lesion was too extensive to allow for a total resection without significant morbidity. The patient died 20 months later as a result of hepatic metastases. This case underscores the importance of surgical resection for this rare spinal tumor.

The present report delineates the complicated postoperative courses of 3 patients with malignant tumors in the upper cervical spine, who had been treated with ion-beam radiotherapy before the index surgery. Ion-beam radiotherapy using proton or carbon particles has been used as an effective adjunctive treatment for various malignant tumors, because it has the physical advantage of a steeper fall-off dose over photon radiotherapy, enabling dose localization in the deep tissues, larger doses per fraction, and fewer overall treatment times.[2,15] Despite these advantages, ion-beam radiotherapy is reportedly associated with several problems including skin erosion, gastrointestinal mucositis, and local recurrence.[15] Our 3 patients developed several postoperative problems, including delayed healing of the retropharyngeal mucosa and submucosal muscles leading to the development of serious deep infections and prolonged dysphagia, possibly attributable to the preoperative ion-beam

radiotherapy that might have damaged the retropharyngeal soft tissues. Basic experiments have demonstrated that radiation inhibits the deposition and remodeling of collagen in surgical wounds by fibroblasts.[16] Such complications should be anticipated after an anterior transoral approach for patients who have previously undergone ion-beam radiotherapy. One treatment option to avoid such complications might be the primary reconstruction of the retropharyngeal wall using a free vascularized musculocutaneous flap or a pectoralis major muscle pedicle flap, as performed in patient 3 during the revision surgery in this study. Neo *et al*[8] reported a patient in whom a chordoma involving C1 was dissected with the deep layer of the retropharyngeal mucosa followed by a primary reconstruction of the retropharyngeal mucosa using a vascularized radial forearm flap, which was anastomosed with the right facial vessels. Another option for avoiding postoperative retropharyngeal problems might be to select an extraoral approach.[7,17]

In conclusion, 3 patients with malignant primary tumors in the upper cervical spine were treated using tumor resection through a combined posterior and anterior approach. In all patients, the gross total resection of the tumors was achieved, but complications associated with disturbances in the healing of the retropharyngeal wall were observed. Preventive methods, such as the primary repair of the retropharyngeal wall using muscular/musculocutaneous flaps, should be considered for patients undergoing tumor resection through a transoral approach after failed ion-beam irradiation.

■ Key Points

- Three cases of malignant tumors in the upper cervical spine were treated surgically by a combination of posterior tumor resection and stabilization and anterior tumor resection through a mandible-splitting approach after failed ion-beam radiation therapy.
- Although the intralesional total resection of the tumors was achieved, all 3 patients developed postoperative complications including deep wound infection, cerebrospinal fluid leakage, infection discitis, and early recurrence.
- The complications were successfully managed by salvage surgery in all patients.
- A preventive method, such as primary repair of the retropharyngeal wall using muscular/musculocutaneous flaps, should be considered for patients who undergo tumor resection through a transoral approach after ion-beam irradiation.

References

1. Noël G, Feuvret L, Calugaru V, et al. Chordomas of the base of the skull and upper cervical spine. One hundred patients irradiated by a 3D conformal technique combining photon and proton beams. *Acta Oncol* 2005;44:700–8.
2. Hug EB, Slater JD. Proton radiation therapy for chordomas and chondrosarcomas of the skull base. *Neurosurg Clin N Am* 2000;11:627–38.
3. Ghogawala Z, Mansfield FL, Borges LF. Spinal radiation before surgical decompression adversely affects outcomes of surgery for symptomatic metastatic spinal cord compression. *Spine* 2001;26:818–24.
4. Gay E, Sekhar LN, Rubinstein E, et al. Chordomas and chondrosarcomas of the cranial base: results and follow-up of 60 patients. *Neurosurgery* 1995;36:887–97.
5. Matsumoto M, Ishii K, Takaishi H, et al. Extensive total spondylectomy for recurrent giant cell tumor in the thoracic spine. Case Report. *J Neurosurg Spine* 2007;6:600–5.
6. Barrenechea IJ, Perin NI, Triana A, et al. Surgical management of chordomas of the cervical spine. *J Neurosurg Spine* 2007;6:398–406.
7. Jiang L, Liu ZJ, Liu XG, et al. Upper cervical spine chordoma of C2–C3. *Eur Spine J* 2009;18:293–300.
8. Neo M, Asato R, Honda K, et al. Transmaxillary and transmandibular approach to a C1 chordoma. *Spine* 2007;32:E236–9.
9. Rhines LD, Fourney DR, Siadati A, et al. En bloc resection of multilevel cervical chordoma with C-2 involvement. Case report and description of operative technique. *J Neurosurg Spine* 2005;2:199–205.
10. Suchomel P, Buchvald P, Barsa P, et al. Single-stage total C-2 intralesional spondylectomy for chordoma with three-column reconstruction. Technical note. *J Neurosurg Spine* 2007;6:611–8.
11. Hall JE, Denis F, Murray J. Exposure of the upper cervical spine for spinal decompression by a mandible and tongue-splitting approach. Case report. *J Bone Joint Surg Am* 1977;59:121–3.
12. Boriani S, Bandiera S, Biagini R, et al. Chordoma of the mobile spine: fifty years of experience. *Spine* 2006;31:493–503.
13. Aquilina K, Lim C, Kamel MH, et al. Epithelioid hemangioendothelioma of the spine. Report of two cases. *J Neurosurg Spine* 2005;3:393–9.
14. Kopniczky Z, Tsimpas A, Lawson DD, et al. Epithelioid hemangioendothelioma of the spine: report of two cases and review of the literature. *Br J Neurosurg* 2008;22:793–7.
15. Tsujii H, Mizoe JE, Kamada T, et al. Overview of clinical experiences on carbon ion radiotherapy at NIRS. *Radiother Oncol* 2004;73(suppl 2):S41–9.
16. Mustoe TA, Porras-Reyes BH. Modulation of wound healing response in chronic irradiated tissues. *Clin Plast Surg* 1993;20:465–72.
17. Carentier A, Blanquet A, George B. Suboccipital and cervical chordomas: radical resection with vertebral artery control. *Neurosurg Focus* 2001;10:E4.

Published April 5, 2010

JEM

Article

The Blimp1–Bcl6 axis is critical to regulate osteoclast differentiation and bone homeostasis

Yoshiteru Miyauchi,[1] Ken Ninomiya,[1] Hiroya Miyamoto,[1] Akemi Sakamoto,[6] Ryotaro Iwasaki,[3] Hiroko Hoshi,[1] Kana Miyamoto,[1] Wu Hao,[1] Shigeyuki Yoshida,[3] Hideo Morioka,[1] Kazuhiro Chiba,[1] Shigeaki Kato,[7] Takeshi Tokuhisa,[6] Mitinori Saitou,[8] Yoshiaki Toyama,[1] Toshio Suda,[4] and Takeshi Miyamoto[1,2,5,9]

[1]Department of Orthopedic Surgery, [2]Department of Integrated Bone Metabolism and Immunology, [3]Department of Dentistry and Oral Surgery, [4]Department of Cell Differentiation, The Sakaguchi Laboratory of Developmental Biology, [5]Keio Kanrinmaru Project, Keio University School of Medicine, Shinjuku-ku, Tokyo 160-8582, Japan
[6]Department of Developmental Genetics, Graduate School of Medicine, Chiba University, Chiba 260-8670, Japan
[7]Institute of Molecular and Cellular Bioscience, University of Tokyo, Bunkyo-ku, Tokyo 113-0032, Japan
[8]Department of Anatomy and Cell Biology, Graduate School of Medicine, Kyoto University, Yoshida-Konoe-cho, Sakyo-ku, Kyoto 606-8501, Japan
[9]Precursory Research for Embryonic Science and Technology, Japan Science and Technology Agency, Kawaguchi, Saitama 332-0012, Japan

Controlling osteoclastogenesis is critical to maintain physiological bone homeostasis and prevent skeletal disorders. Although signaling activating nuclear factor of activated T cells 1 (NFATc1), a transcription factor essential for osteoclastogenesis, has been intensively investigated, factors antagonistic to NFATc1 in osteoclasts have not been characterized. Here, we describe a novel pathway that maintains bone homeostasis via two transcriptional repressors, B cell lymphoma 6 (Bcl6) and B lymphocyte–induced maturation protein-1 (Blimp1). We show that Bcl6 directly targets 'osteoclastic' molecules such as NFATc1, cathepsin K, and dendritic cell-specific transmembrane protein (DC-STAMP), all of which are targets of NFATc1. Bcl6-overexpression inhibited osteoclastogenesis in vitro, whereas Bcl6-deficient mice showed accelerated osteoclast differentiation and severe osteoporosis. We report that Bcl6 is a direct target of Blimp1 and that mice lacking Blimp1 in osteoclasts exhibit osteopetrosis caused by impaired osteoclastogenesis resulting from Bcl6 up-regulation. Indeed, mice doubly mutant in Blimp1 and Bcl6 in osteoclasts exhibited decreased bone mass with increased osteoclastogenesis relative to osteoclast-specific Blimp1-deficient mice. These results reveal a Blimp1–Bcl6–osteoclastic molecule axis, which critically regulates bone homeostasis by controlling osteoclastogenesis and may provide a molecular basis for novel therapeutic strategies.

CORRESPONDENCE
Takeshi Miyamoto:
miyamoto@sc.itc.keio.ac.jp

Abbreviations used: Bcl6, B cell lymphoma 6; Blimp1, B lymphocyte–induced maturation protein 1; BMM, BM macrophage; ChIP, chromatin immunoprecipitation; cKO, conditional KO; Ctsk, cathepsin K; DC-STAMP, DC-specific transmembrane protein; DKO, double KO; NFATc1, nuclear factor of activated T cells 1; PGC, primordial germ cell; RANKL, receptor activator of NF-κB ligand; TRAP, tartrate-resistant acid phosphatase.

Osteoclasts are responsible for bone resorption, and thereby play an essential role in maintaining bone volume and homeostasis (Karsenty and Wagner, 2002). Dysregulation of osteoclast differentiation or function disrupts maintenance of bone homeostasis, which in turn leads to pathogenic conditions such as osteoporosis, rheumatoid arthritis, lytic bone metastases, or Paget's bone disease (Rodan and Martin, 2000). Thus, osteoclasts could potentially be targeted therapeutically to treat skeletal disorders. Osteoclasts originate from BM–derived monocyte/macrophage precursor cells of hematopoietic origin and are differentiated by signaling through the receptor activator of NF-κB ligand (RANKL; Kong et al., 1999). RANKL induces osteoclast differentiation by activating the nuclear factor of activated T cells 1 (NFATc1),

Y. Miyauchi and K. Ninomiya contributed equally to this paper.

The Rockefeller University Press $30.00
J. Exp. Med. Vol. 207 No. 4 751-762
www.jem.org/cgi/doi/10.1084/jem.20091957

Published April 5, 2010

a transcription factor required for osteoclastogenesis (Takayanagi et al., 2002; Koga et al., 2004; Sato et al., 2006; Shinohara et al., 2008). Activated NFATc1 induces expression of "osteoclastic" molecules essential for osteoclast differentiation and function, such as DC-specific transmembrane protein (DC-STAMP) to facilitate cell–cell fusion, cathepsin K (Ctsk) to promote bone matrix proteolysis, and NFATc1 to drive differentiation (Yagi et al., 2005; Li et al., 2006). Thus, signaling pathways mediated by positive regulators of NFATc1 in osteoclastogenesis have been intensively studied, whereas factors negatively modulating osteoclastogenesis are largely unknown.

B lymphocyte–induced maturation protein 1 (Blimp1) has been investigated in numerous cell types (John and Garrett-Sinha, 2009) and is reportedly essential for specification and maintenance of primordial germ cells (PGCs) through silencing of somatic programs (Ohinata et al., 2005). B cell lymphoma 6 (Bcl6) was originally identified as a protooncogene because its chromosomal translocation and constitutive expression promotes lymphomagenesis (Ohno, 2006). *Bcl6*$^{-/-}$ mice show impaired germinal center formation (Fukuda et al., 1997). The roles of Blimp1 and Bcl6 have also been investigated in B cell and plasma cell development (Turner et al., 1994; Fukuda et al., 1997), as well as in T cells (Dent et al., 1998; Kusam et al., 2003; Ichii et al., 2004; Kallies et al., 2006; Martins et al., 2006; Cimmino et al., 2008). However, the roles of Blimp1 and Bcl6, both of which are transcriptional repressors, have not previously been characterized in osteoclastogenesis or skeletal disorders, although mutations in Bcl6-associated molecules are reportedly seen in skeletal pathologies such as malformation of fingers and clavicles (Ng et al., 2004). Recently, it was reported that inhibiting NFATc1 using the NFATc1 inhibitor FK506 actually resulted in reduced bone mass caused by inhibition of bone formation that was more potent than inhibition of osteoclastogenesis (Koga et al., 2005). Therefore, additional regulators of osteoclast differentiation have been sought as factors that could potentially increase bone mass.

In this study, we identify two transcriptional repressors controlling osteoclastogenesis, Bcl6 and Blimp1. We show that Bcl6 negatively regulates expression of osteoclastic genes, i.e., *NFATc1*, *DC-STAMP*, and *Ctsk*, which are all NFATc1 targets. We found that Bcl6 is recruited to promoters of these genes, and that Bcl6 inhibits osteoclastogenesis. We also report that Blimp1 binds to the *Bcl6* promoter, likely suppressing its expression. Bcl6-deficient mice exhibited decreased bone mass with increased osteoclastogenesis, whereas osteoclast-specific Blimp1 conditional KO (cKO) mice showed impaired osteoclast differentiation and increased bone mass, likely resulting from Bcl6 dysregulation. Overall, our data demonstrate that an axis of transcriptional repressors is crucial to regulate osteoclastogenesis and bone homeostasis.

RESULTS

Bcl6 is a negative regulator of osteoclastogenesis

RANKL stimulates osteoclastogenesis by activating NFATc1 (Takayanagi et al., 2002; Koga et al., 2004; Sato et al., 2006; Shinohara et al., 2008). To identify genes potentially suppressed after RANKL stimulation of osteoclast precursor cells (BM macrophages [BMMs]), we undertook comparative microarray screens of BMMs treated with or without RANKL and found that expression of the transcriptional repressor *Bcl6* was down-regulated by RANKL (Fig. 1 A). *Bcl6* down-regulation by RANKL was confirmed by real-time RT-PCR, immunofluorescence, and immunoblot analysis (Fig. S1 and Fig. 1 B). Immunofluorescence analysis showed that Bcl6 was detected in the nuclei of M-CSF–dependent macrophages, but not in nuclei of multinuclear osteoclasts induced by RANKL (Fig. 1 B). Interestingly, chromatin immunoprecipitation (ChIP) assays showed that, in the absence of RANKL, Bcl6 was recruited to the *NFATc1* P1 promoter, a region critical for regulating *NFATc1* expression in osteoclasts, and was dismissed from the promoter after RANKL treatment. In contrast, NFATc1, an essential positive regulator of osteoclastogenesis, was absent from the *NFATc1* P1 promoter in the absence of RANKL, but recruited after RANKL stimulation (Fig. 1 C). These results suggest a potential role of Bcl6 in inhibiting osteoclastogenesis. Bcl6 overexpression also potently inhibited osteoclast differentiation in vitro (Fig. 1 D), suggesting that Bcl6 negatively regulates osteoclast differentiation and that its down-regulation after RANKL stimulation is critical to induce osteoclastogenesis.

Bcl6 deficiency facilitates osteoclast formation

To characterize the physiological roles of Bcl6 in osteoclastogenesis, we analyzed Bcl6-deficient (*Bcl6*$^{-/-}$) mice. *Bcl6*$^{-/-}$ mice exhibited lower bone mass as detected by microradiographical and dual-energy x-ray absorptiometry analysis compared with heterozygous littermates (*Bcl6*$^{+/-}$; Fig. 2, A and B). Consistently, histomorphometric analysis of *Bcl6*$^{-/-}$ mice demonstrated increased osteoclastogenesis and large osteoclast formation in *Bcl6*$^{-/-}$ mice. *Bcl6*$^{-/-}$ mice also showed elevated levels of serum C-terminal telopeptides of type I collagen (CTx) and decreased bone parameters (Fig. 2, C and D, and Fig. S2). In vitro, osteoclast progenitor cells isolated from Bcl6-deficient mice and treated with RANKL differentiated more rapidly into multinuclear tartrate-resistant acid phosphatase (TRAP)–positive cells than did those from control mice (Fig. 2 E and not depicted). Lower concentrations of RANKL not sufficient to differentiate control cells induced osteoclast differentiation of Bcl6-deficient cells (Fig. 2 E). Furthermore, increased bone resorbing activity was evident in Bcl6-deficient osteoclasts (Fig. 2 F), suggesting loss of a negative regulator of osteoclast function and differentiation. Deletion of Bcl6 in osteoclast precursor cells did not alter cell proliferation or induce apoptosis (Fig. S3). Thus, Bcl6 functions to regulate osteoclast differentiation and bone homeostasis, and its down-regulation by RANKL is required for osteoclast formation.

Blimp1 regulates Bcl6 expression and osteoclastogenesis

Next, we searched for a factor that might suppress Bcl6 during osteoclastogenesis and found that the transcriptional

Published April 5, 2010

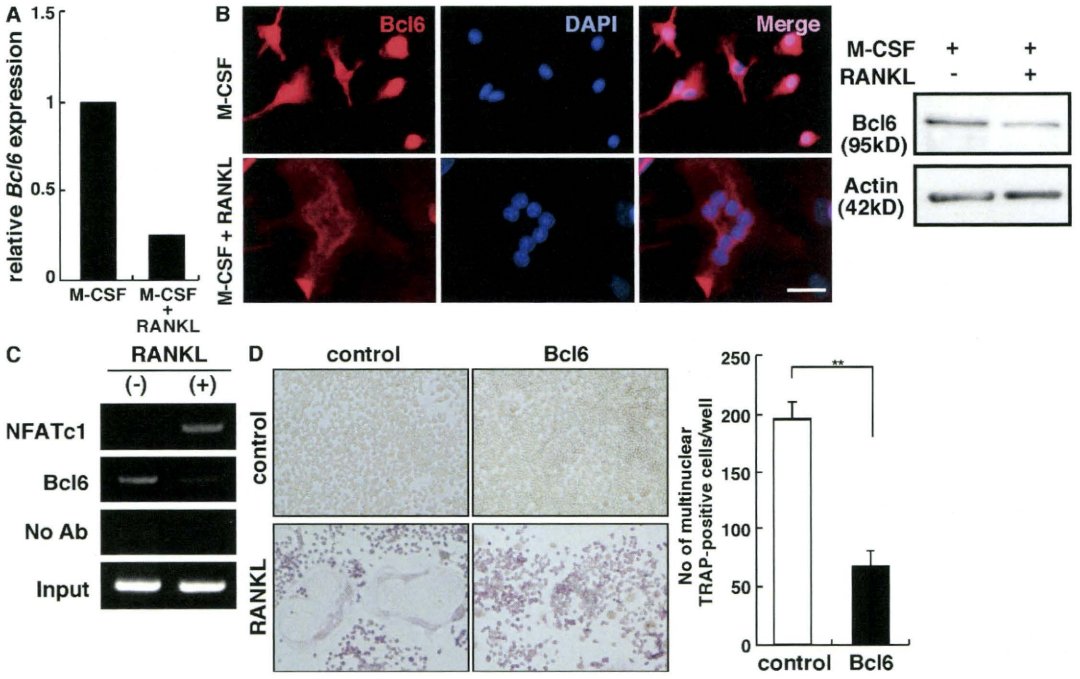

Figure 1. Bcl6 is suppressed during osteoclastogenesis and inhibits osteoclast formation. (A) *Bcl6* expression was examined by comparative microarray analysis between osteoclast precursors (M-CSF) and osteoclasts (M-CSF + RANKL) cultured for 6 d. (B) BMMs were cultured with or without RANKL for 8 d and subjected to immunofluorescence staining (left) and immunoblot (right) for Bcl6. Nuclei were visualized by DAPI. Bar, 25 µm. (C) Recruitment of NFATc1 and Bcl6 to the *NFATc1* P1 distal promoter was detected by ChIP assay. RAW264.7 cells were stimulated with or without RANKL for 48 h and subjected to ChIP analysis. (D) RAW264.7 cells transduced with Bcl6-overexpressing (Bcl6) or mock (control) retrovirus were cultured in the presence (RANKL) or absence (control) of RANKL for 5 d and stained with TRAP. Left, TRAP staining. (right) Numbers are means ± SD of multinuclear TRAP-positive cells in control or Bcl6-overexpressing RAW264.7 cells cultured with RANKL (**, $P < 0.001$; $n = 6$). Representative data of three independent experiments are shown (B–D).

repressor *Blimp1*, also called *Prdm1*, was specifically upregulated during osteoclast formation (Fig. S4 A). Blimp1 expression in osteoclasts was also demonstrated by using Blimp1-EGFP BAC transgenic mice, in which the EGFP sequence is knocked into the *Blimp1* locus, and by the observation that TRAP-positive cells showed Blimp1 expression (Fig. S4 B). RT-PCR analysis confirmed *Blimp1* induction in BMMs in the presence of RANKL in parallel with induction of *Ctsk*, a marker of osteoclast differentiation (Fig. 3 A). To determine whether Bcl6 is a Blimp1 target, an electrophoretic mobility shift assay (EMSA) was undertaken using a Bcl6 probe corresponding to a *Bcl6* regulatory region (Cimmino et al., 2008). Blimp1 formed a complex with the probe, but not with a Bcl6mut probe in which two nucleotides are changed to disrupt the Blimp1 binding sequence (Fig. S5 A). The PRDI probe, which corresponds to a region of the *interferon β* promoter known to bind Blimp1 protein (Keller and Maniatis, 1991) weakly but competitively, inhibited complex formation of the Bcl6 probe with Blimp1 (Fig. S5 A). In addition, unlabeled Bcl6 probe competed with labeled Bcl6 probe–Blimp1 to block complex formation, whereas unlabeled Bcl6mut probe did not (Fig. S5 A), confirming specificity and suggesting that Bcl6 is a direct Blimp1 target. Furthermore, ChIP analysis showed that, in the absence of RANKL, Blimp1 was absent from the *Bcl6* promoter, but was recruited there by RANKL treatment (Fig. S5 B). Thus, we conclude that Bcl6 is a direct target of Blimp1 in osteoclasts.

To investigate physiological roles of Blimp1 in osteoclast differentiation, we established osteoclast-specific Blimp1 cKO mice ($Ctsk^{Cre/+}Blimp1^{flox/-}$), as Blimp1-null mice are embryonic lethal (Vincent et al., 2005). Blimp1 heterozygotes ($Blimp1^{+/-}$) were crossed with Ctsk-Cre mice ($Ctsk^{Cre/+}$) in which *Cre* is knocked into the *Ctsk* locus (Nakamura et al., 2007). Next, $Ctsk^{Cre/+}Blimp1^{+/-}$ mice were crossed with a transgenic strain harboring *loxP*-flanked (floxed) *Blimp1* alleles ($Blimp1^{flox/flox}$; Ohinata et al., 2005) to yield Blimp1 cKO mice. $Ctsk^{Cre/+}Blimp1^{flox/+}$ mice served as controls. Blimp1 cKO mice showed increased trabecular bone mass and an expanded growth plate compared with control mice, as seen by histomorphometric and microradiographical analysis (Fig. 3, B–D). TRAP staining of bone sections and analysis of serum CTx levels demonstrated severe inhibition of TRAP-positive osteoclast formation and bone resorbing activity, respectively (Fig. 3, E and F). Bone-morphometric analysis revealed reduced osteoblastic parameters in Blimp1 cKO mice (Fig. 3 C). Differentiation of osteoblasts isolated from osteoclast-specific Blimp1 cKO mice did not differ

Published April 5, 2010

from that seen in control mice (Fig. S6), suggesting that Blimp1 deficiency in osteoclast progenitor cells promotes decreased osteoblast differentiation and bone formation. Deletion of Blimp1 in osteoclasts did not alter precursor cell proliferation or induction of apoptosis (Fig. S7, A and B). Furthermore, immune cell populations such as CD3-, B220-,

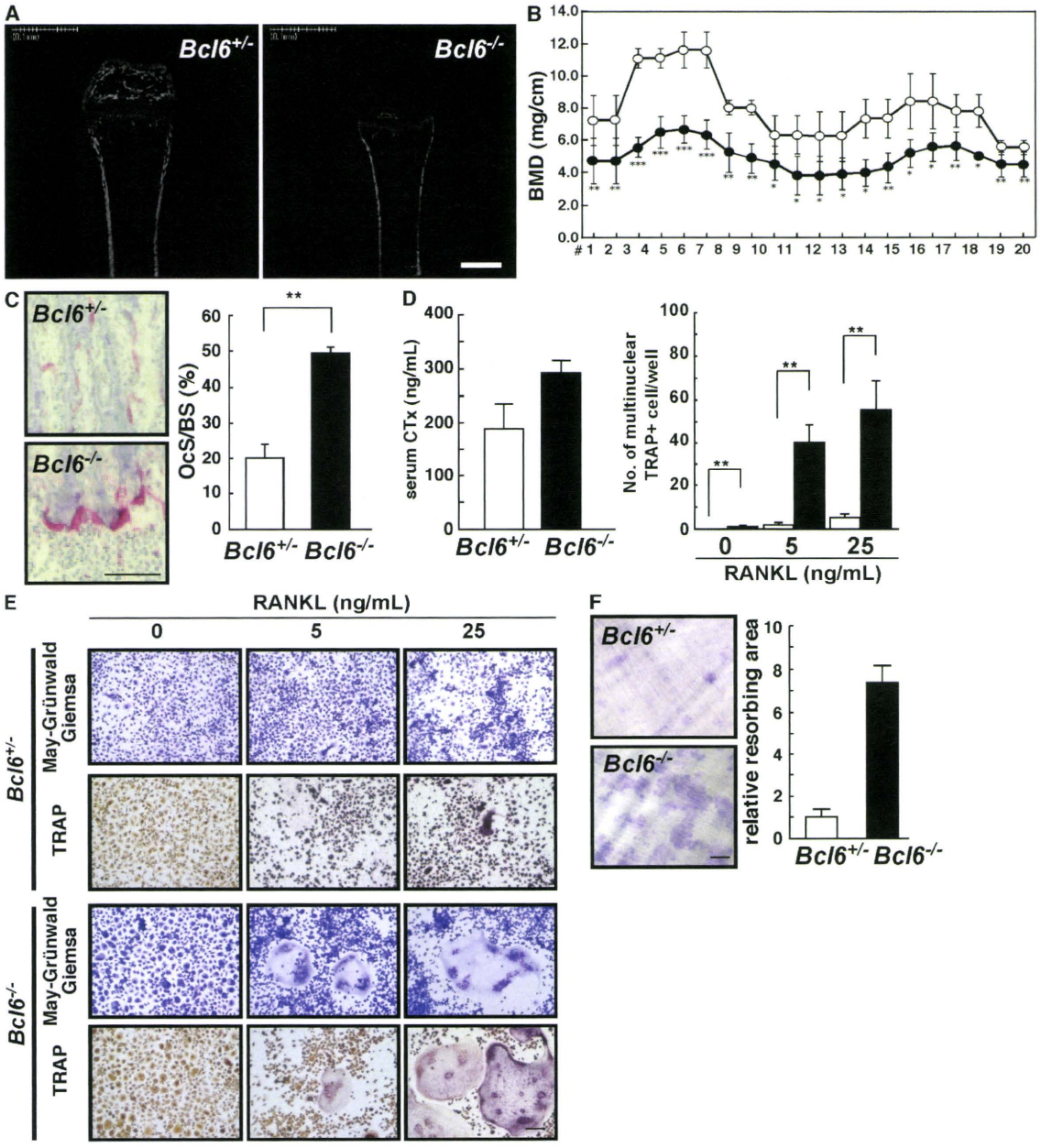

Figure 2. Increased osteoclast formation resulting from Bcl6 deficiency. (A) Micro focus CT analysis of femurs of *Bcl6*$^{+/-}$ (left) and *Bcl6*$^{-/-}$ (right) mice. (B) Bone mineral density (BMD) of equal longitudinal division of femurs of *Bcl6*$^{+/-}$ (open circles) and *Bcl6*$^{-/-}$ (closed circles) mice. Data are mean BMD (mg/cm^2) ± SD (*, $P < 0.05$; **, $P < 0.01$; ***, $P < 0.001$; $n = 3$). (C) TRAP staining of tibial sections of *Bcl6*$^{+/-}$ (top) and *Bcl6*$^{-/-}$ (bottom) mice, and osteoclast surface as a percentage of bone surface (OcS/BS). Data are means ± SD (**, $P < 0.001$; $n = 5$). (D) Serum levels of C-terminal teropeptides of type I collagen (CTx) were analyzed in *Bcl6*$^{+/-}$ (white bar) and *Bcl6*$^{-/-}$ (shaded bar) mice. Data are means ± SD (**, $P < 0.001$; $n = 3$). (E) Osteoclast precursor cells from control (*Bcl6*$^{+/-}$) or *Bcl6*$^{-/-}$ mice were cultured in the presence or absence of RANKL for 5 d and subjected to May-Grünwald Giemsa and TRAP staining, and the number of multinuclear TRAP-positive cells containing more than three nuclei was determined. Data are means ± SD of cells containing more than three nuclei (**, $P < 0.001$; $n = 3$). (F) Bone resorbing activity in *Bcl6*$^{+/-}$ (top) and *Bcl6*$^{-/-}$ (bottom) osteoclasts was analyzed by a pit formation assay. Representatives of at least three (E) and two (F) independent experiments are shown. Bars: (A) 1 mm; (C, E, and F) 100 µm.

Mac1-, or Gr1-positive cells were normal in the Blimp1 osteoclast-specific KO, suggesting that Blimp1 is required to regulate osteoclast differentiation and bone homeostasis (Fig. S8).

Severe inhibition of osteoclastogenesis was also observed in in vitro culture. Multinuclear TRAP-positive osteoclast formation induced by RANKL was significantly inhibited in Blimp1 cKO cells (Fig. 4, A and B). *Blimp1* expression was significantly up-regulated in the presence of RANKL in control cells; however, *Blimp1* induction was significantly inhibited in Blimp1 cKO cells (Fig. 4 C). In contrast, *Bcl6* expression was significantly down-regulated in control cells in the presence of RANKL; however, *Bcl6* expression in Blimp1 cKO cells was significantly up-regulated in Blimp1 cKO cells, even in the presence of RANKL (Fig. 4, C and D),

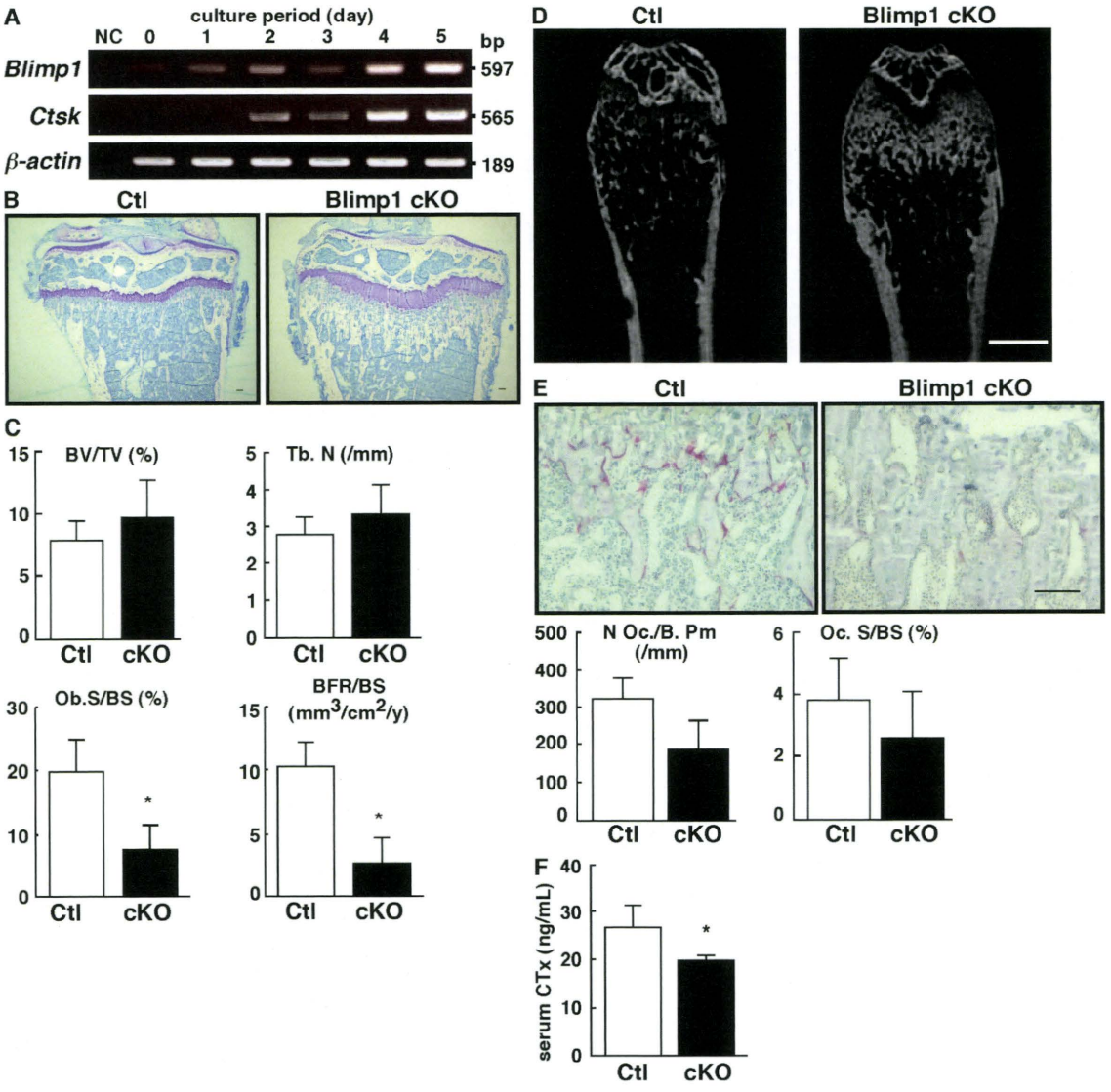

Figure 3. Blimp1 is essential for osteoclastogenesis and regulates bone homeostasis. (A) Total RNA isolated from BMMs cultured with M-CSF and RANKL for indicated periods was subjected to RT-PCR analysis with primers specific for *Blimp1* (top), *Ctsk* (middle), and *β-actin* (bottom). Representatives of at least three independent experiments are shown. (B–F) Bone phenotypes of osteoclast-specific Blimp1 KO (Blimp1 cKO) female mice at 8 wk old. (B) Longitudinal sections of tibias of control mice (Ctl; left) and Blimp1 cKO mice (right) were stained by toluidine blue. (C) Bone parameters are shown. Data are mean bone volume per total volume (BV/TV; %), trabecular number (Tb. N; /mm), osteoblast surface per bone surface (Ob.S/BS; %), or bone formation rate per bone surface (BFR/BS; $mm^3/cm^2/y$) ± SD of control (Ctl; white bar) and Blimp1 cKO (cKO; shaded bar) mice (*, $P < 0.01$; $n = 5$). (D) Microfocus CT analysis of femurs of control mice (Ctl; left) and Blimp1 cKO mice (right). (E) TRAP staining of tibial sections of control mice (Ctl; left) and Blimp1 cKO mice (right). Osteoclast parameters are shown as mean osteoclast number per bone perimeter (N.Oc/B.Pm) or osteoclast surface per bone surface (Oc.S/BS.) ± SD of control (Ctl; white bar) and Blimp1 cKO (cKO; shaded bar) mice ($n = 5$). (F) Serum CTx levels as a marker of bone resorption of control (Ctl; white bar) and Blimp1 cKO (cKO; shaded bar) mice (*, $P < 0.01$; $n = 5$). Bars: (B and E) 100 µm; (D) 1 mm.

Published April 5, 2010

JEM

suggesting that Blimp1 is critical to suppress *Bcl6* expression in osteoclasts during differentiation by RANKL and is essential for regulating osteoclastogenesis.

Bcl6 suppresses NFATc1 target genes during osteoclastogenesis

Expression of genes encoding osteoclastic factors, such as *NFATc1*, *DC-STAMP*, and *Ctsk*, all of which are targets of NFATc1 (Matsumoto et al., 2004; Asagiri et al., 2005; Yagi et al., 2007), was markedly inhibited in Blimp1 cKO osteoclasts (Fig. 5 A). It was shown by ChIP analysis that NFATc1 was not evident on osteoclastic gene promoters without RANKL, but was recruited there after RANKL treatment of control cells (Fig. 5 B). In contrast, in the absence of RANKL, Bcl6 was present on osteoclastic gene promoters, but was lost from those promoters after RANKL treatment of control

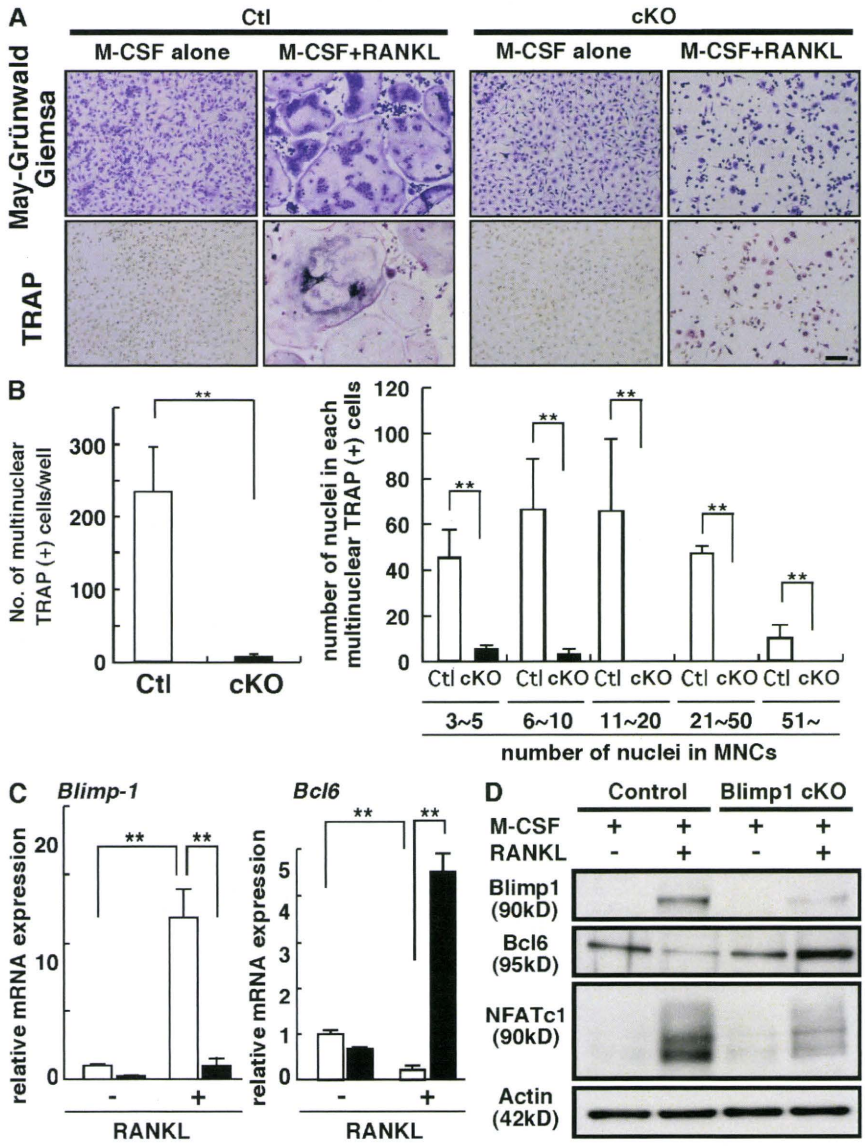

Figure 4. Impaired osteoclastogenesis and Bcl6 expression resulting from Blimp1 deficiency. (A–C) BMMs from control (Ctl) or Blimp1 cKO (cKO) mice were cultured in the presence or absence of RANKL for 8 d. Cells were then subjected to May-Grünwald Giemsa and TRAP staining (A), the number of TRAP-positive cells containing more than three nuclei was scored (B, left), and the number of nuclei in each multinuclear osteoclast was determined (B, right). Bar, 100 µm. Numbers are means ± SD of multinuclear cells (**, $P < 0.001$; $n = 3$). (C) Total RNA was prepared from control (white bars) or Blimp1 cKO (shaded bars) cells treated with (+) or without (−) RANKL, and *Blimp1* (left) or *Bcl6* (right) expression relative to *β-actin* was analyzed by quantitative real-time PCR. Data represent means ± SD of *Blimp1*/*β-actin* or *Bcl6*/*β-actin* levels (**, $P < 0.001$; $n = 4$). (D) Whole-cell lysates from control or Blimp1 cKO cells cultured with M-CSF alone or M-CSF plus RANKL were analyzed by immunoblotting to detect Blimp1, Bcl6, and NFATc1. Actin was analyzed as an internal control. Representatives of at least four independent experiments are shown.

Published April 5, 2010

cells (Fig. 5 B). These data strongly indicate that NFATc1 and Bcl6 are reciprocally recruited to osteoclastic gene promoters. Significantly, reciprocal recruitment of NFATc1 and Bcl6 was severely impaired in Blimp1 cKO cells (Fig. 5 B), suggesting that Blimp1 up-regulation is critical for loss of Bcl6 from osteoclastic promoters after RANKL stimulation. Bcl6 was not present on the *NFATc2* promoter, which is not activated by RANKL stimulation (Asagiri et al., 2005), in the presence or absence of RANKL (Fig. 5 B), suggesting that Bcl6 is selectively recruited to promoters of osteoclastic genes and inhibits osteoclast differentiation. Whereas Bcl6 was down-regulated by RANKL treatment in control cells, Bcl6 expression was maintained in Blimp1 cKO cells, even in the presence of RANKL (Fig. 4 C and Fig. S9). These data indicate that impaired Bcl6 down-regulation caused by loss of Blimp1 results in continuous inhibition of osteoclastic gene expression, which in turn promotes severe inhibition of osteoclastogenesis and increased bone mass.

Finally, to confirm the role of Blimp1 in regulating osteoclastogenesis through Bcl6, osteoclast-specific Blimp1/Bcl6 double KO mice (double KO [DKO]; $Ctsk^{Cre/+}Blimp1^{flox/-}Bcl6^{-/-}$ mice) were established (Fig. 6). DKO mice exhibited decreased bone mass in vivo compared with Blimp1 cKO mice (Fig. 6 A). Similarly, progenitor cells isolated from DKO mice showed accelerated osteoclastogenesis compared with those from Blimp1 cKO mice (Fig. 6, B and C), suggesting that Blimp1 regulates osteoclastogenesis in part through controlling Bcl6. These results reveal that the Blimp1–Bcl6–osteoclastic molecule axis is critical for controlling osteoclast differentiation and bone homeostasis (Fig. 7).

DISCUSSION

Here, we show that two transcriptional repressors, Bcl6 and Blimp1, are essential to control physiological osteoclast development and maintenance of bone homeostasis. Bcl6, a member of the POZ/BTB-zinc finger protein family, suppresses expression of "osteoclastic" genes, all of which are targets of NFATc1 (Matsumoto et al., 2004; Asagiri et al., 2005; Yagi et al., 2007), thereby antagonizing NFATc1 function. Indeed, NFATc1 deficiency in osteoclasts results in impaired differentiation (Asagiri et al., 2005), whereas Bcl6-deficient mice exhibit accelerated osteoclast formation and decreased bone mass. Blimp1, encoded by *Prdm1*, acts as a suppressor of Bcl6, likely by direct binding to the *Bcl6* promoter. In contrast to Bcl6-deficient mice, osteoclast-specific Blimp1 cKO mice display impaired osteoclast differentiation and increased bone mass. Expression of *Bcl6* and *Blimp1* is reciprocal in normal osteoclast formation, and unusual elevation

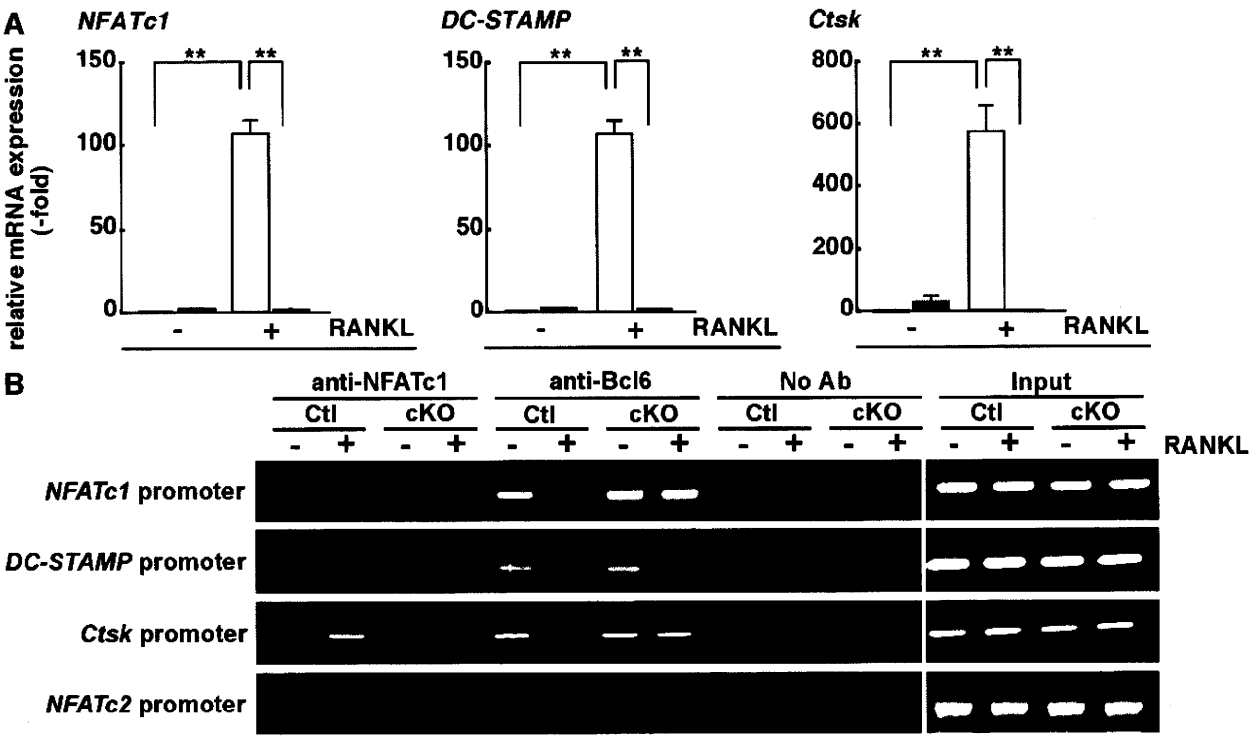

Figure 5. Bcl6 suppresses osteoclast differentiation. (A) Total RNA was prepared from control (white bars) or Blimp1 cKO (shaded bars) cells treated with (+) or without (−) RANKL, and the expression of the osteoclastic genes *NFATc1*, *DC-STAMP*, and *Ctsk* relative to *β-actin* was analyzed by a quantitative real-time PCR. Data are means ± SD of *osteoclastic genes/β-actin*. (**, $P < 0.001$; $n = 4$). (B) Recruitment of NFATc1 and Bcl6 to promoters of osteoclastic genes such as *NFATc1*, *DC-STAMP*, *Ctsk*, or a negative control gene *NFATc2* was analyzed by a ChIP assay. Representatives of at least four (A) or two (B) independent experiments are shown.

Published April 5, 2010

JEM

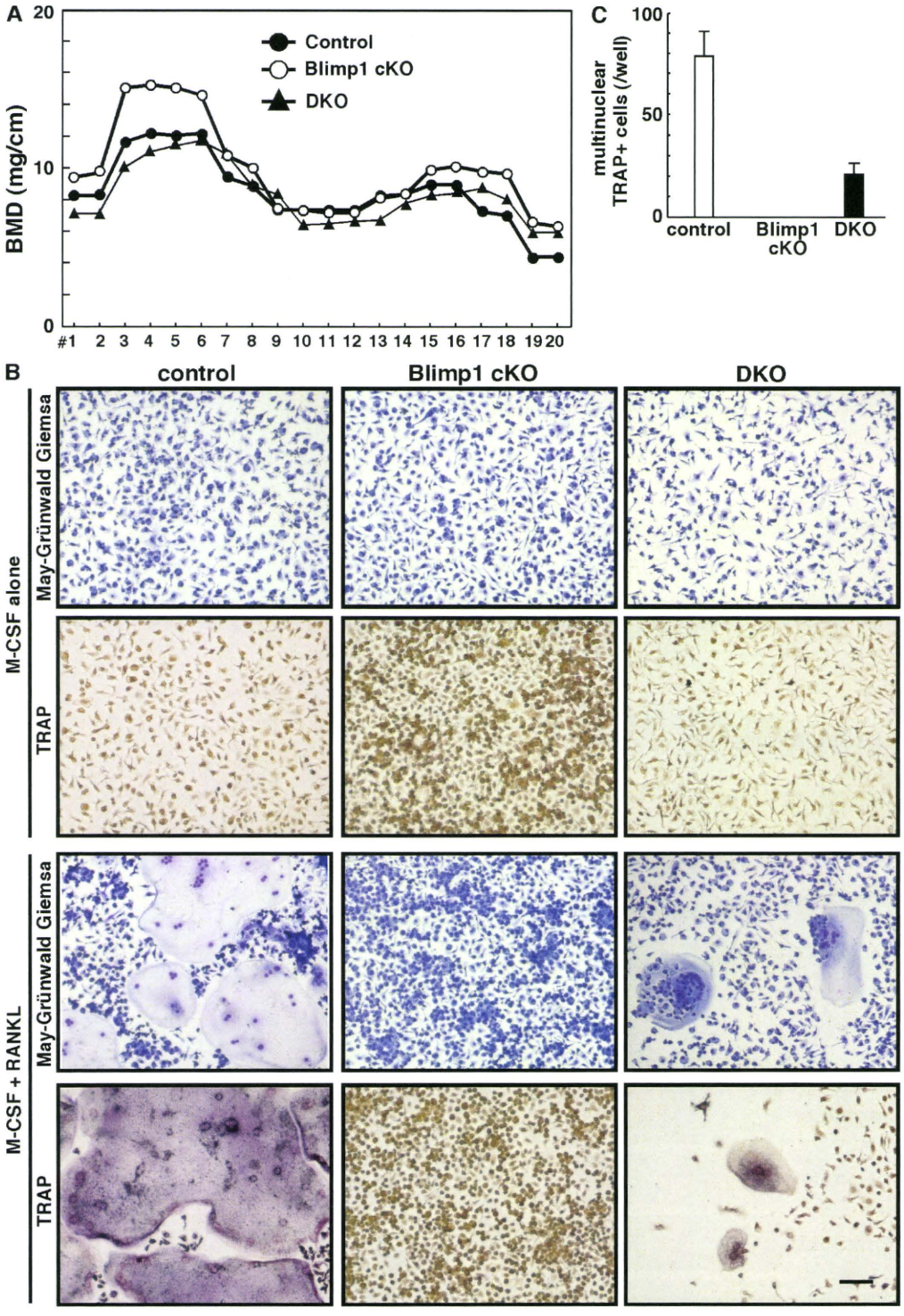

Figure 6. Bcl6 is a target of Blimp1 during osteoclastogenesis. (A) Bone mineral density (BMD) of equal longitudinal division of femurs of control (filled circles), Blimp1 cKO (open circles), and Blimp1 cKO/Bcl6 KO (DKO; filled triangles) mice. Data represent mean BMD ($n = 4$). (B and C) Osteoclast progenitor cells from control, Blimp1 cKO or DKO mice were cultured in the presence of M-CSF alone or M-CSF plus RANKL for 8 d. Cells were then subjected to May-Grünwald Giemsa and TRAP staining (B), and the number of TRAP-positive cells containing more than three nuclei was scored (C). Results are representative of three independent experiments. Bar, 100 µm.

Published April 5, 2010

of *Bcl6* expression caused by Blimp1 deficiency leads to osteoclastogenesis failure, as indicated by increased bone mass seen in a Blimp1 cKO model. Signals positively regulating NFATc1 in osteoclasts, such as TRAF6, c-Fos, ITAM-PLCγ-Ca^{2+} signals, Btk, and Tec (Takayanagi et al., 2002; Koga et al., 2004; Shinohara et al., 2008), have been characterized, and NFATc1 reportedly positively autoregulates in osteoclasts (Asagiri et al., 2005). However, factors modulating this activity have not been described. Our study characterizes such an axis of factors that serve as a molecular switch to control osteoclastogenesis and bone homeostasis after RANKL stimulation.

To date, the skeletal and immune systems have been shown to share common molecules to achieve homeostasis (Nakashima and Takayanagi, 2008). RANKL and RANK were originally identified in T cells and DCs (Anderson et al., 1997), respectively, and both are essential for osteoclastogenesis (Kong et al., 1999; Dougall et al., 1999). NFATc1 was identified in T cells and plays an essential role in osteoclast formation (Northrop et al., 1994; Asagiri et al., 2005). DC-STAMP plays a role in DC function and is required for cell–cell fusion of osteoclasts and macrophage giant cells (Yagi et al., 2005, 2007; Sawatani et al., 2008). Besides roles in immune system, Bcl6 has antiapoptotic and protooncogenic function

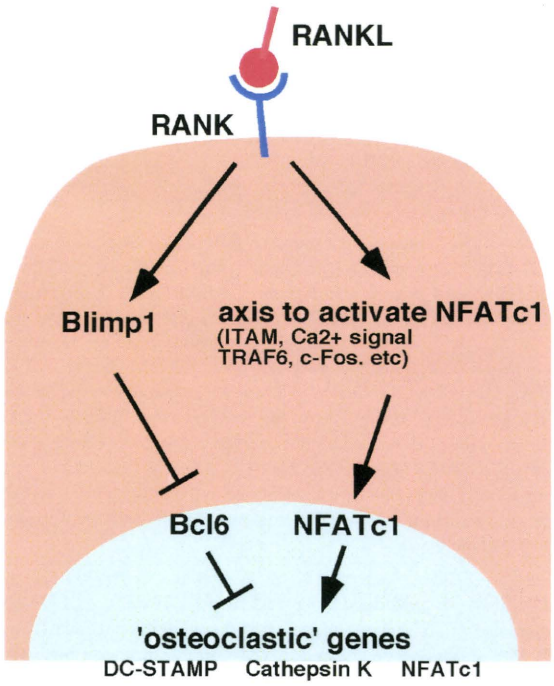

Figure 7. A schematic model of osteoclastogenesis regulated by the Blimp1–Bcl6–osteoclastic gene axis. RANKL–RANK interaction results in Blimp1 induction, leading to Bcl6 down-regulation and dissociation of Bcl6 from osteoclastic gene promoters, an event critical for osteoclastogenesis. NFATc1 activation is induced by various factors, such as ITAM, TRAF6, c-Fos, and Ca^{2+} signaling, which are also activated by RANKL.

(Baron et al., 2002; Ohno, 2006). Blimp1 also functions in specification of the germ cell lineage and acts as a tumor suppressor (Ohinata et al., 2005; John and Garrett-Sinha, 2009). Here, we show that Bcl6 and Blimp1, which are both implicated in B cell and T cell development (Turner et al., 1994; Fukuda et al., 1997; Dent et al., 1998; Kusam et al., 2003; Ichii et al., 2004; Kallies et al., 2006; Martins et al., 2006; Cimmino et al., 2008), have a novel function in regulating osteoclastogenesis and maintenance of bone homeostasis. It has been reported that Blimp1 represses Bcl6 (Cimmino et al., 2008) or that Blimp1 and Bcl6 regulate each other (Shapiro-Shelef and Calame, 2005). Blimp1 expression was reportedly inhibited by Bcl6 (Martins et al., 2006); however, we did not detect dysregulation of Blimp1 expression in Bcl6-deficient osteoclasts (unpublished data). Osteoclast-specific Blimp1/Bcl6 DKO mice exhibited increased osteoclastogenesis with decreased bone mass compared with Blimp1 cKO mice, indicating that Blimp1 regulates Bcl6 in osteoclasts. However, although Bcl6-deficient cells showed accelerated osteoclastogenesis compared with control cells, DKO cells showed decreased osteoclast differentiation compared with control cells, suggesting that Blimp1 regulates osteoclastogenesis through Bcl6 along with other target molecules. Blimp1 has multiple targets in lymphocytes and PGCs (Shaffer et al., 2002; Kurimoto et al., 2008), and thus it is possible that Blimp1 has multiple targets in osteoclasts as well. In osteoclasts, several negative regulators for osteoclastogenesis, such as *Id*, *Mafb*, and *Irf8*, have been identified (Lee et al., 2006; Kim et al., 2007; Zhao et al., 2009). Blimp1 may also target these molecules in osteoclasts to stimulate osteoclast differentiation. Further investigations are needed to clarify the molecular mechanisms of the regulation of osteoclastogenesis by Blimp1.

We used $Ctsk^{Cre/+}$ mice to establish osteoclast-specific Blimp1 cKO mice because $Ctsk^{Cre/+}$ mice have been used to generate osteoclast-specific KOs of factors such as the estrogen receptor and Bcl-XL (Nakamura et al., 2007; Iwasawa et al., 2009). Osteoclastogenesis, including *Ctsk* expression, has been evaluated in osteoclast-specific gene-targeted cells (Nakamura et al., 2007). *Blimp1* expression is induced earlier than *Ctsk* (Fig. 3 A), and osteoclastogenesis is inhibited in Blimp1 cKO cells, suggesting that continuous Blimp1 expression is required for full osteoclast differentiation under control of RANKL. Blimp1 is also known to be induced by BMP4 and LIF in PGCs, where it functions as a transcriptional repressor (Ohinata et al., 2009). In osteoclasts, Blimp1 is induced by RANKL and acts to repress Bcl6. Thus, signaling regulating Blimp1 expression differs between PGCs and osteoclasts.

Bone homeostasis requires a delicate balance between osteoclastic and osteoblastic activities. A decline in bone volume is closely related to up-regulation of osteoclast activity, and thus osteoclasts could be targeted therapeutically to treat skeletal disorders such as osteoporosis and destructive bone metastasis. FK506, a specific inhibitor of calcineurin-NFATs, inhibits osteoclastogenesis, but does not increase bone mass, as FK506 also inhibits bone formation (Koga et al., 2005). Thus, additional factors that could negatively regulate osteoclast

Published April 5, 2010

JEM

differentiation, such as those identified here, have been sought. Thus, our study provides new insight into regulation of osteoclastogenesis and bone homeostasis and forms the basis for developing novel therapeutic approaches to treat skeletal disorders.

MATERIALS AND METHODS

Mice. *Bcl6* $^{-/-}$ mice on a mixed C57BL/6 X 129/Sv background were generated by crossing *Bcl6* heterozygotes (*Bcl6*$^{+/-}$; Fukuda et al., 1997). Osteoclast-specific Blimp1 cKO mice on a C57BL/6 background were generated from three lines: mice carrying *loxP*-flanked *Blimp1* alleles (*Blimp1*$^{flox/flox}$; Ohinata et al., 2005), mice harboring *Cre* in the *Ctsk* (*Ctsk*$^{Cre/+}$) locus (Nakamura et al., 2007), and *Blimp1* heterozygotes (*Blimp1*$^{+/-}$; provided by A. Tarakhovsky, The Rockefeller University, New York, NY). Animals were maintained under specific pathogen–free conditions in animal facilities certified by the Keio University School of Medicine animal care committee. Animal protocols were approved by the Keio University School of Medicine animal care committee.

In vitro osteoclast formation. BM cells isolated from long bones (femurs, tibias, and humerus) were cultured 72 h in αMEM (Sigma-Aldrich) containing 10% heat-inactivated FBS (JRH Biosciences) and GlutaMax supplemented with M-CSF (50 ng/ml; Kyowa Hakko Kirin Co.). Adherent cells were then collected for analysis. 10^5 cells were cultured with M-CSF and recombinant soluble RANKL (25 ng/ml; PeproTech Ltd.) for indicated time periods. Mouse spleen cells were cultured overnight in αMEM containing 10% heat-inactivated FBS and GlutaMax supplemented with M-CSF. After this incubation, nonadherent cells were collected and 10^5 cells were cultured with M-CSF and recombinant soluble RANKL (5 or 25 ng/ml) for the indicated time periods. Osteoclastogenesis was evaluated by TRAP and May-Grünwald Giemsa staining (Miyamoto et al., 2000; Yagi et al., 2005). RAW264.7 cells were maintained in αMEM containing 10% heat-inactivated FBS and GlutaMax and stimulated by recombinant soluble RANKL to induce osteoclast formation.

Pit formation assay. Bone resorbing activity of osteoclasts was analyzed as previously described (Iwamoto et al., 2004). In brief, osteoclast precursors isolated from indicated mice were seeded on dentin slices and cultured in the presence of M-CSF plus RANKL for 6 d. Dentin slices were then stained by toluidine blue and observed under a microscope (model BZ-9000; Keyence Co.).

Analysis of skeletal morphology. Bcl6 $^{-/-}$, DKO, and control littermates were necropsied 16 d after birth. Hindlimbs were removed, fixed with 70% ethanol, and subjected to dual-energy x-ray absorptiometry analysis to measure bone mineral density and for bone-histomorphometric analysis. Female 8-wk-old Blimp1 cKO mice and control littermates were administered intraperitoneal injections of 16 mg/kg calcein (Dojindo Co.) at 6 and 1 d before sacrifice to evaluate bone formation rate. Hindlimbs were removed and analyzed as described above.

ELISA. Serum levels of osteocalcin and C-terminal telopeptides of type I collagen (CTx) were measured by the Mouse Osteocalcin EIA kit (Biomedical Technologies Inc.) and RatLaps EIA (Immunodiagnostics Systems Ltd.), respectively. Assays were undertaken following the manufacturers' instructions.

Real-time PCR analysis. Total RNAs were isolated from BM cultures by TRIzol reagent (Invitrogen). After denaturation of total RNAs at 70°C for 5 min, cDNAs were synthesized from total RNAs using oligo(dT) primer and reverse transcription (Wako Pure Chemicals Industries). Real-time PCR was performed using SYBR Premix ExTaq II (Takara Bio Inc.) with the DICE Thermal cycler (Takara Bio Inc.), according to the manufacturer's instructions. Samples were matched to a standard curve generated by amplifying serially diluted products using the same PCR reactions. *β-actin* expression served as an internal control. Primer sequences were as follows: *β-actin* forward: 5′-TGAGAGGGAAATCGTGCGTGAC-3′; *β-actin* reverse: 5′-AAGAAGGAAGGCTGGAAAAGAG-3′; *Bcl6* forward: 5′-AGACGCACAGTGACAAACCATACAA-3′; *Bcl6* reverse: 5′-GCTCCACAAATGTTACAGCGATAGG-3′; *Blimp1* forward: 5′-TTCTTGTGTGGTATTGTCGGGACTT-3′; *Blimp1* reverse: 5′-TTGGGGACACTCTTTGGGTAGAGTT-3′; *Ctsk* forward: 5′-ACGGAGGCATTGACTCTGAAGATG-3′; *Ctsk* reverse: 5′-GGAAGCACCAACGAGAGGAGAAAT-3′; *DC-STAMP* forward: 5′-TCCTCCATGAACAAACAGTTCCAA-3′; *DC-STAMP* reverse: 5′-AGACGTGGTTTAGGAATGCAGCTC-3′; *NFATc1* forward: 5′-CAAGTCTCACCACAGGGCTCACTA-3′; *NFATc1* reverse: 5′-GCGTGAGAGGTTCATTCTCCAAGT-3′; *type I collagen* forward: 5′-CCTGGTAAAGATGGTGCC-3′; *type I collagen* reverse: 5′-CACCAGGTTCACCTTTCGCACC-3′; *osteocalcin* forward: 5′-TAGCAGACACCATGAGGACCCT-3′; *osteocalcin* reverse: 5′-TGGACATGAAGGCTTTGTCAGA-3′.

Immunofluoresence. Cells were fixed with 4% paraformaldehyde (Wako Pure Chemical Industries) in PBS solution for 15 min at room temperature. After washing to remove fixation solution, cells were permeabilized in PBS containing 0.1% Triton X-100 for 10 min at room temperature and then washed. Nonspecific antibody binding was blocked by treatment with 5% BSA (Sigma-Aldrich Co.) in PBS. Cells were then stained with anti-Bcl6 antibody (1:50 dilution, N-3; Santa Cruz Biotechnology, Inc.) at 4°C overnight, washed with PBS and stained with Alexa Fluor 546–conjugated anti-rabbit IgG antibody (1:200 dilution) for 1 h at room temperature. Cells were washed to remove secondary antibody and incubated with DAPI solution (Dojindo Co.; 1:5,000) for nuclear staining, followed by microscopic observation (model BZ-9000; Keyence Co).

Immunoblotting analysis. Whole-cell lysates were prepared from BM cultures using RIPA buffer (1% Triton X-100, 1% sodium deoxycholate, 0.1% SDS, 150 mM NaCl, 10 mM Tris-HCl, pH 7.5, 5 mM EDTA, and a protease inhibitor cocktail; Sigma-Aldrich). Equivalent amounts of protein were separated by SDS-PAGE and transferred to a PVDF membrane (Millipore). Proteins were detected using the following antibodies: anti-NFATc1 (7A6), anti-Blimp1 (6D3), anti-Bcl6 (N-3) (Santa Cruz Biotechnology, Inc.), and anti-actin (A2066; Sigma-Aldrich).

EMSA. Nuclear extracts were prepared from COS7 cells transfected with pCAG-HA-Blimp1 or pCAG. Each extract was incubated for 30 min on ice with a [^{32}P]labeled probe in binding buffer (10 mM Tris-HCl, pH 7.9, 50 mM NaCl, 0.5 mM EDTA, 1 mM DTT, and 10% glycerol) containing 2 μg of poly(dI-dC), KCl, and BSA. Complexes were separated on 5% polyacrylamide gels in TGE buffer (25 mM Tris-HCl, 190 mM glycine, and 1 mM EDTA). The Bcl6 probe corresponding to a putative Blimp1 binding site in the *Bcl6* gene was 5′-AGGTTTCATAGGAAGTGAAAACCCTGCTAT-3′. A mutated probe (underlined residues) served as a negative control (Bcl6mut probe; 5′-AGGTTTCATAGGAAGTTAGAACCCTGCTAT-3′). After electrophoresis, gels were dried and exposed to the imaging plate, and signals were analyzed using ImageGauge software on the BAS2000 image analyzer (Fuji Film Co.).

ChIP. ChIP was performed on osteoclasts. M-CSF–induced BMMs were cultured on 100-mm type I collagen-coated culture dishes (Asahi Glass Co.) with M-CSF and recombinant RANKL for the indicated time periods, and then subjected to ChIP analysis using the ChIP-IT Enzymatic kit (ActivMotif Inc.), according to the manufacturer's instructions. Immunoprecipitation was performed using anti-NFATc1 (7A6), anti-Bcl6 (N-3), and anti-Blimp1 (C14A4; Cell Signaling Technology). DNA was purified by QIAquick PCR purification kit (QIAGEN) and analyzed using primers corresponding to the following promoters: *NFATc1*-P1 promoter, 5′-CCGGGACGCCCATGCAATCTGTTAGTAATT-3′ (sense) and 5′-GCGGGTGCCCTGAGAAAGCTACTCTCCCTT-3′ (antisense); the *DC-STAMP* promoter, 5′-GGGGGTCCTCATTTCTACAACTCAT-3′

(sense) and 5′-GCCACATCACCCTGAATCAATCTT-3′ (antisense); the *Ctsk* promoter, 5′-CCTTAAACTGGCTCCTGTCAAAGA-3′ (sense) and 5′-CCCTTCTTCAGAAGCCCTGTAAT-3′ (antisense); *NFATc2* promoter, 5′-TTATCAGGGAGCACTGCCCATCTCCGCTTT-3′ (sense) and 5′-CGGTCTGGCCTGAGCGACAGGCCCAGACAA-3′ (antisense); and *Bcl6* promoter, 5′-CAGCCACCCTGAGTTTACAA-3′ (sense) and 5′-CGTTCCAGCACTGTTTTGAA-3′ (antisense).

Microarray analysis. BM cells were isolated from 8-wk-old mouse and cultured in the presence of M-CSF for 3 d. M-CSF–dependent adherent cells were harvested and cultured with M-CSF alone for macrophages and M-CSF plus RANKL for osteoclasts, respectively. After 6 days of cultivation, total RNA was isolated and microarray analysis was undertaken using GeneChip Mouse Genome 430 2.0 Array (Affymetrix). Data were analyzed using GeneChip Operating Software and deposited in Minimum Information about a Microarray Experiment compliant in Gene Expression Omnibus (GEO accession no. GSE20850).

Online supplemental material. Fig. S1 shows that *Bcl6* is transcriptionally repressed by RANKL. Fig. S2 shows bone parameters of $Bcl6^{+/-}$ and $Bcl6^{-/-}$ mice. Fig. S3 shows proliferation and apoptosis of osteoclast precursors from $Bcl6^{+/-}$ and $Bcl6^{-/-}$ mice. Fig. S4 shows Blimp1 expression in osteoclasts. Fig. S5 shows that Blimp1 binds to the Bcl6 promoter. Fig. S6 shows normal osteoblastic differentiation in Blimp1 cKO cells. Fig. S7 shows proliferation and apoptosis of osteoclast precursors from Blimp1 cKO and control mice. Fig. S8 shows immune cell populations in spleens of Blimp1 cKO and control mice. Fig. S9 shows dysregulation of Bcl6 in Blimp1 cKO BMM. Online supplemental material is available at http://www.jem.org/cgi/content/full/jem.20091957/DC1.

We thank Y. Sato for technical support. We thank Prof. T. Kitamura (University of Tokyo) and Prof. A. Tarakhovsky (Rockefeller University) for providing retroviral vectors and $Blimp1^{+/-}$ mice, respectively.

T. Miyamoto was supported by a grant-in-aid for Young Scientists, Precursory Research for Embryonic Science and Technology (PREST), the Uehara memorial foundation, Takeda Science Foundation, The Nakatomi Foundation, and Keio Kanrinmaru project, Japan. Y. Miyauchi was supported by a grant-in-aid for Young Scientists.

The authors have no conflicting financial interests.

Submitted: 8 September 2009
Accepted: 10 March 2010

REFERENCES

Anderson, D.M., E. Maraskovsky, W.L. Billingsley, W.C. Dougall, M.E. Tometsko, E.R. Roux, M.C. Teepe, R.F. DuBose, D. Cosman, and L. Galibert. 1997. A homologue of the TNF receptor and its ligand enhance T-cell growth and dendritic-cell function. *Nature.* 390:175–179. doi:10.1038/36593

Asagiri, M., K. Sato, T. Usami, S. Ochi, H. Nishina, H. Yoshida, I. Morita, E.F. Wagner, T.W. Mak, E. Serfling, and H. Takayanagi. 2005. Autoamplification of NFATc1 expression determines its essential role in bone homeostasis. *J. Exp. Med.* 202:1261–1269. doi:10.1084/jem.20051150

Baron, B.W., J. Anastasi, M.J. Thirman, Y. Furukawa, S. Fears, D.C. Kim, F. Simone, M. Birkenbach, A. Montag, A. Sadhu, et al. 2002. The human programmed cell death-2 (PDCD2) gene is a target of BCL6 repression: implications for a role of BCL6 in the down-regulation of apoptosis. *Proc. Natl. Acad. Sci. USA.* 99:2860–2865. doi:10.1073/pnas.042702599

Cimmino, L., G.A. Martins, J. Liao, E. Magnusdottir, G. Grunig, R.K. Perez, and K.L. Calame. 2008. Blimp-1 attenuates Th1 differentiation by repression of ifng, tbx21, and bcl6 gene expression. *J. Immunol.* 181:2338–2347.

Dent, A.L., J. Hu-Li, W.E. Paul, and L.M. Staudt. 1998. T helper type 2 inflammatory disease in the absence of interleukin 4 and transcription factor STAT6. *Proc. Natl. Acad. Sci. USA.* 95:13823–13828. doi:10.1073/pnas.95.23.13823

Dougall, W.C., M. Glaccum, K. Charrier, K. Rohrbach, K. Brasel, T. De Smedt, E. Daro, J. Smith, M.E. Tometsko, C.R. Maliszewski, et al. 1999. RANK is essential for osteoclast and lymph node development. *Genes Dev.* 13:2412–2424. doi:10.1101/gad.13.18.2412

Fukuda, T., T. Yoshida, S. Okada, M. Hatano, T. Miki, K. Ishibashi, S. Okabe, H. Koseki, S. Hirosawa, M. Taniguchi, et al. 1997. Disruption of the Bcl6 gene results in an impaired germinal center formation. *J. Exp. Med.* 186:439–448. doi:10.1084/jem.186.3.439

Ichii, H., A. Sakamoto, Y. Kuroda, and T. Tokuhisa. 2004. Bcl6 acts as an amplifier for the generation and proliferative capacity of central memory CD8+ T cells. *J. Immunol.* 173:883–891.

Iwamoto, K., T. Miyamoto, N. Hosogane, I. Hamaguchi, M. Takami, K. Takagi, and T. Suda. 2004. Dimer formation of receptor activator of nuclear factor kappa B induces incomplete osteoclast formation. *Biochem. Biophys. Res. Commun.* 325:229–234. doi:10.1016/j.bbrc.2004.10.024

Iwasawa, M., T. Miyazaki, Y. Nagase, T. Akiyama, Y. Kadono, M. Nakamura, Y. Oshima, T. Yasui, T. Matsumoto, T. Nakamura, et al. 2009. The antiapoptotic protein Bcl-xL negatively regulates the bone-resorbing activity of osteoclasts in mice. *J. Clin. Invest.* 119:3149–3159.

John, S.A., and L.A. Garrett-Sinha. 2009. Blimp1: a conserved transcriptional repressor critical for differentiation of many tissues. *Exp. Cell Res.* 315:1077–1084. doi:10.1016/j.yexcr.2008.11.015

Kallies, A., E.D. Hawkins, G.T. Belz, D. Metcalf, M. Hommel, L.M. Corcoran, P.D. Hodgkin, and S.L. Nutt. 2006. Transcriptional repressor Blimp-1 is essential for T cell homeostasis and self-tolerance. *Nat. Immunol.* 7:466–474. doi:10.1038/ni1321

Karsenty, G., and E.F. Wagner. 2002. Reaching a genetic and molecular understanding of skeletal development. *Dev. Cell.* 2:389–406. doi:10.1016/S1534-5807(02)00157-0

Keller, A.D., and T. Maniatis. 1991. Identification and characterization of a novel repressor of beta-interferon gene expression. *Genes Dev.* 5:868–879. doi:10.1101/gad.5.5.868

Kim, K., J.H. Kim, J. Lee, H.M. Jin, H. Kook, K.K. Kim, S.Y. Lee, and N. Kim. 2007. MafB negatively regulates RANKL-mediated osteoclast differentiation. *Blood.* 109:3253–3259. doi:10.1182/blood-2006-09-048249

Koga, T., M. Inui, K. Inoue, S. Kim, A. Suematsu, E. Kobayashi, T. Iwata, H. Ohnishi, T. Matozaki, T. Kodama, et al. 2004. Costimulatory signals mediated by the ITAM motif cooperate with RANKL for bone homeostasis. *Nature.* 428:758–763. doi:10.1038/nature02444

Koga, T., Y. Matsui, M. Asagiri, T. Kodama, B. de Crombrugghe, K. Nakashima, and H. Takayanagi. 2005. NFAT and Osterix cooperatively regulate bone formation. *Nat. Med.* 11:880–885. doi:10.1038/nm1270

Kong, Y.Y., H. Yoshida, I. Sarosi, H.L. Tan, E. Timms, C. Capparelli, S. Morony, A.J. Oliveira-dos-Santos, G. Van, A. Itie, et al. 1999. OPGL is a key regulator of osteoclastogenesis, lymphocyte development and lymph-node organogenesis. *Nature.* 397:315–323. doi:10.1038/16852

Kurimoto, K., Y. Yabuta, Y. Ohinata, M. Shigeta, K. Yamanaka, and M. Saitou. 2008. Complex genome-wide transcription dynamics orchestrated by Blimp1 for the specification of the germ cell lineage in mice. *Genes Dev.* 22:1617–1635. doi:10.1101/gad.1649908

Kusam, S., L.M. Toney, H. Sato, and A.L. Dent. 2003. Inhibition of Th2 differentiation and GATA-3 expression by BCL-6. *J. Immunol.* 170:2435–2441.

Lee, J., K. Kim, J.H. Kim, H.M. Jin, H.K. Choi, S.H. Lee, H. Kook, K.K. Kim, Y. Yokota, S.Y. Lee, et al. 2006. Id helix-loop-helix proteins negatively regulate TRANCE-mediated osteoclast differentiation. *Blood.* 107:2686–2693. doi:10.1182/blood-2005-07-2798

Li, C.Y., K.J. Jepsen, R.J. Majeska, J. Zhang, R. Ni, B.D. Gelb, and M.B. Schaffler. 2006. Mice lacking cathepsin K maintain bone remodeling but develop bone fragility despite high bone mass. *J. Bone Miner. Res.* 21:865–875. doi:10.1359/jbmr.060313

Martins, G.A., L. Cimmino, M. Shapiro-Shelef, M. Szabolcs, A. Herron, E. Magnusdottir, and K. Calame. 2006. Transcriptional repressor Blimp-1 regulates T cell homeostasis and function. *Nat. Immunol.* 7:457–465. doi:10.1038/ni1320

Matsumoto, M., M. Kogawa, S. Wada, H. Takayanagi, M. Tsujimoto, S. Katayama, K. Hisatake, and Y. Nogi. 2004. Essential role of p38 mitogen-activated protein kinase in cathepsin K gene expression during

osteoclastogenesis through association of NFATc1 and PU.1. *J. Biol. Chem.* 279:45969–45979. doi:10.1074/jbc.M408795200

Miyamoto, T., F. Arai, O. Ohneda, K. Takagi, D.M. Anderson, and T. Suda. 2000. An adherent condition is required for formation of multinuclear osteoclasts in the presence of macrophage colony-stimulating factor and receptor activator of nuclear factor kappa B ligand. *Blood.* 96:4335–4343.

Nakamura, T., Y. Imai, T. Matsumoto, S. Sato, K. Takeuchi, K. Igarashi, Y. Harada, Y. Azuma, A. Krust, Y. Yamamoto, et al. 2007. Estrogen prevents bone loss via estrogen receptor alpha and induction of Fas ligand in osteoclasts. *Cell.* 130:811–823. doi:10.1016/j.cell.2007.07.025

Nakashima, T., and H. Takayanagi. 2008. The dynamic interplay between osteoclasts and the immune system. *Arch. Biochem. Biophys.* 473:166–171. doi:10.1016/j.abb.2008.04.004

Ng, D., N. Thakker, C.M. Corcoran, D. Donnai, R. Perveen, A. Schneider, D.W. Hadley, C. Tifft, L. Zhang, A.O. Wilkie, et al. 2004. Oculofaciocardiodental and Lenz microphthalmia syndromes result from distinct classes of mutations in BCOR. *Nat. Genet.* 36:411–416. doi:10.1038/ng1321

Northrop, J.P., S.N. Ho, L. Chen, D.J. Thomas, L.A. Timmerman, G.P. Nolan, A. Admon, and G.R. Crabtree. 1994. NF-AT components define a family of transcription factors targeted in T-cell activation. *Nature.* 369:497–502. doi:10.1038/369497a0

Ohinata, Y., B. Payer, D. O'Carroll, K. Ancelin, Y. Ono, M. Sano, S.C. Barton, T. Obukhanych, M. Nussenzweig, A. Tarakhovsky, et al. 2005. Blimp1 is a critical determinant of the germ cell lineage in mice. *Nature.* 436:207–213. doi:10.1038/nature03813

Ohinata, Y., H. Ohta, M. Shigeta, K. Yamanaka, T. Wakayama, and M. Saitou. 2009. A signaling principle for the specification of the germ cell lineage in mice. *Cell.* 137:571–584. doi:10.1016/j.cell.2009.03.014

Ohno, H. 2006. Pathogenetic and clinical implications of non-immunoglobulin; BCL6 translocations in B-cell non-Hodgkin's lymphoma. *J. Clin. Exp. Hematop.* 46:43–53. doi:10.3960/jslrt.46.43

Rodan, G.A., and T.J. Martin. 2000. Therapeutic approaches to bone diseases. *Science.* 289:1508–1514. doi:10.1126/science.289.5484.1508

Sato, K., A. Suematsu, T. Nakashima, S. Takemoto-Kimura, K. Aoki, Y. Morishita, H. Asahara, K. Ohya, A. Yamaguchi, T. Takai, et al. 2006. Regulation of osteoclast differentiation and function by the CaMK-CREB pathway. *Nat. Med.* 12:1410–1416. doi:10.1038/nm1515

Sawatani, Y., T. Miyamoto, S. Nagai, M. Maruya, J. Imai, K. Miyamoto, N. Fujita, K. Ninomiya, T. Suzuki, R. Iwasaki, et al. 2008. The role of DC-STAMP in maintenance of immune tolerance through regulation of dendritic cell function. *Int. Immunol.* 20:1259–1268. doi:10.1093/intimm/dxn082

Shaffer, A.L., K.I. Lin, T.C. Kuo, X. Yu, E.M. Hurt, A. Rosenwald, J.M. Giltnane, L. Yang, H. Zhao, K. Calame, and L.M. Staudt. 2002. Blimp-1 orchestrates plasma cell differentiation by extinguishing the mature B cell gene expression program. *Immunity.* 17:51–62. doi:10.1016/S1074-7613(02)00335-7

Shapiro-Shelef, M., and K. Calame. 2005. Regulation of plasma-cell development. *Nat. Rev. Immunol.* 5:230–242. doi:10.1038/nri1572

Shinohara, M., T. Koga, K. Okamoto, S. Sakaguchi, K. Arai, H. Yasuda, T. Takai, T. Kodama, T. Morio, R.S. Geha, et al. 2008. Tyrosine kinases Btk and Tec regulate osteoclast differentiation by linking RANK and ITAM signals. *Cell.* 132:794–806. doi:10.1016/j.cell.2007.12.037

Takayanagi, H., S. Kim, T. Koga, H. Nishina, M. Isshiki, H. Yoshida, A. Saiura, M. Isobe, T. Yokochi, J. Inoue, et al. 2002. Induction and activation of the transcription factor NFATc1 (NFAT2) integrate RANKL signaling in terminal differentiation of osteoclasts. *Dev. Cell.* 3:889–901. doi:10.1016/S1534-5807(02)00369-6

Turner, C.A. Jr., D.H. Mack, and M.M. Davis. 1994. Blimp-1, a novel zinc finger-containing protein that can drive the maturation of B lymphocytes into immunoglobulin-secreting cells. *Cell.* 77:297–306. doi:10.1016/0092-8674(94)90321-2

Vincent, S.D., N.R. Dunn, R. Sciammas, M. Shapiro-Shalef, M.M. Davis, K. Calame, E.K. Bikoff, and E.J. Robertson. 2005. The zinc finger transcriptional repressor Blimp1/Prdm1 is dispensable for early axis formation but is required for specification of primordial germ cells in the mouse. *Development.* 132:1315–1325. doi:10.1242/dev.01711

Yagi, M., T. Miyamoto, Y. Sawatani, K. Iwamoto, N. Hosogane, N. Fujita, K. Morita, K. Ninomiya, T. Suzuki, K. Miyamoto, et al. 2005. DC-STAMP is essential for cell-cell fusion in osteoclasts and foreign body giant cells. *J. Exp. Med.* 202:345–351. doi:10.1084/jem.20050645

Yagi, M., K. Ninomiya, N. Fujita, T. Suzuki, R. Iwasaki, K. Morita, N. Hosogane, K. Matsuo, Y. Toyama, T. Suda, and T. Miyamoto. 2007. Induction of DC-STAMP by alternative activation and downstream signaling mechanisms. *J. Bone Miner. Res.* 22:992–1001. doi:10.1359/jbmr.070401

Zhao, B., M. Takami, A. Yamada, X. Wang, T. Koga, X. Hu, T. Tamura, K. Ozato, Y. Choi, L.B. Ivashkiv, et al. 2009. Interferon regulatory factor-8 regulates bone metabolism by suppressing osteoclastogenesis. *Nat. Med.* 15:1066–1071. doi:10.1038/nm.2007